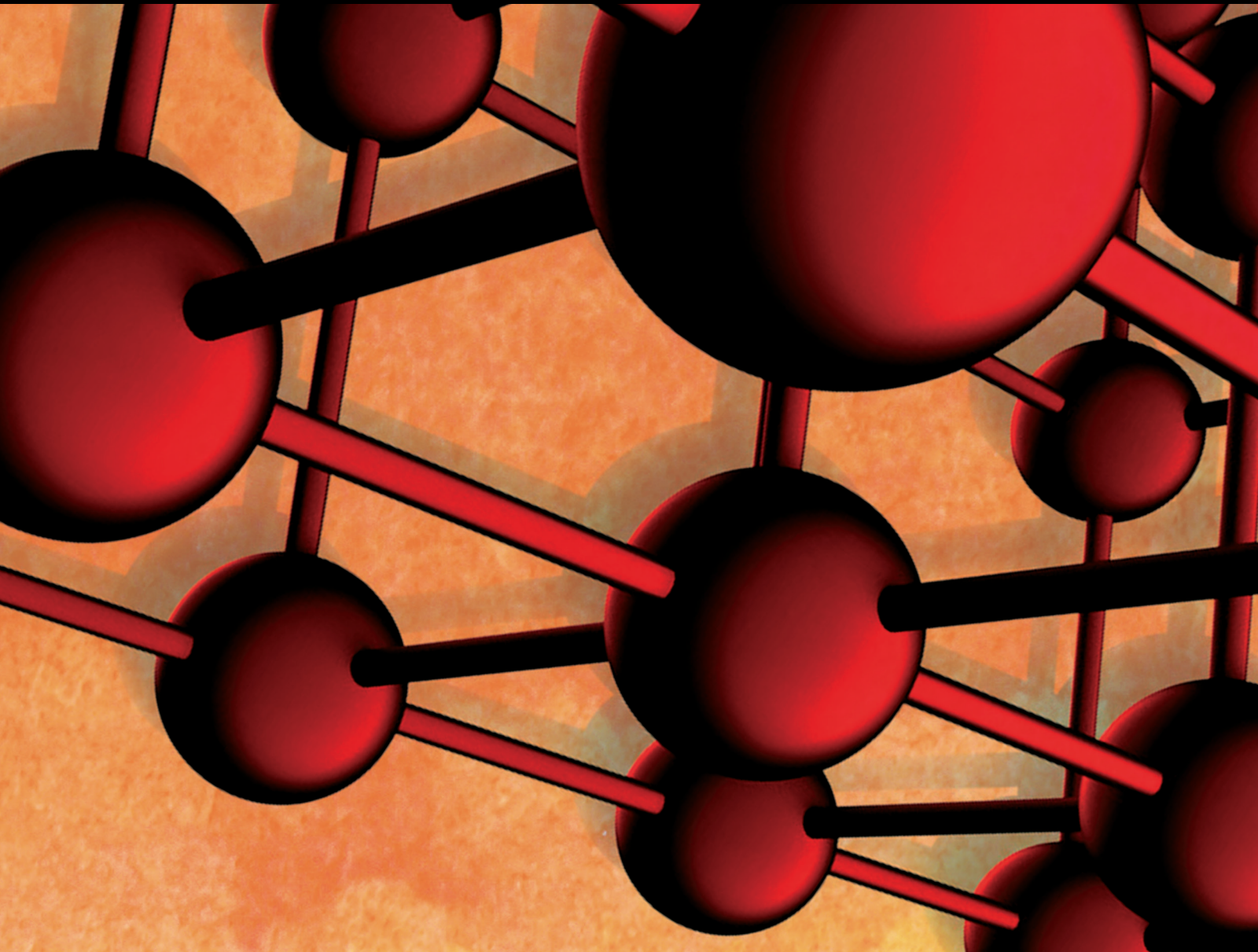


Advances in Materials Science and Engineering

Fiber-Reinforced Cement Composites: Mechanical Properties and Structural Implications 2020

Lead Guest Editor: Doo-Yeol Yoo

Guest Editors: Nemkumar Banthia, Kazunori Fujikake, Young H. Kim, and Rishi Gupta





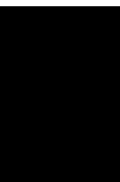
**Fiber-Reinforced Cement Composites:
Mechanical Properties and Structural
Implications 2020**

Advances in Materials Science and Engineering

**Fiber-Reinforced Cement Composites:
Mechanical Properties and Structural
Implications 2020**

Lead Guest Editor: Doo-Yeol Yoo


Guest Editors: Nemkumar Banthia, Kazunori
Fujikake, Young H. Kim, and Rishi Gupta



Copyright © 2020 Hindawi Limited. All rights reserved.

This is a special issue published in "Advances in Materials Science and Engineering." All articles are open access articles distributed under the Creative Commons Attribution License, which permits unrestricted use, distribution, and reproduction in any medium, provided the original work is properly cited.

Chief Editor

















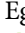

Amit Bandyopadhyay , USA

Associate Editors

Vamsi Balla , India
Mitun Das , USA
Sandip Harimkar, USA
Ravi Kumar , India
Peter Majewski , Australia
Enzo Martinelli , Italy
Luigi Nicolais , Italy
Carlos R. Rambo , Brazil
Michael J. Schütze , Germany
Kohji Tashiro , Japan
Zhonghua Yao , China
Dongdong Yuan , China
Wei Zhou , China

Academic Editors

Antonio Abate , Germany
Hany Abdo , Saudi Arabia
H.P.S. Abdul Khalil , Malaysia
Ismael Alejandro Aguayo Villarreal ,
Mexico
Sheraz Ahmad , Pakistan
Michael Aizenshtein, Israel
Jarir Aktaa, Germany
Bandar AlMangour, Saudi Arabia
Huaming An, China
Alicia Esther Ares , Argentina
Siva Avudaiappan , Chile
Habib Awais , Pakistan
NEERAJ KUMAR BHOI, India
Enrico Babilio , Italy
Renal Backov, France
M Bahubalendruni , India
Sudharsan Balasubramanian , India
Markus Bambach, Germany
Irene Bavasso , Italy
Stefano Bellucci , Italy
Brahim Benmokrane, Canada
Jean-Michel Bergheau , France
Guillaume Bernard-Granger, France
Giovanni Berselli, Italy
Patrice Berthod , France
Michele Bianchi , Italy
Hugo C. Biscaia , Portugal

Antonio Boccaccio, Italy
Mohamed Bououdina , Saudi Arabia
Gianlorenzo Bussetti , Italy
Antonio Caggiano , Germany
Marco Cannas , Italy
Qi Cao, China
Gianfranco Carotenuto , Italy
Paolo Andrea Carraro , Italy
Jose Cesar de Sa , Portugal
Wen-Shao Chang , United Kingdom
Qian Chen , China
Francisco Chinesta , France
Er-Yuan Chuang , Taiwan
Francesco Colangelo, Italy
María Criado , Spain
Enrique Cuan-Urquiza , Mexico
Lucas Da Silva , Portugal
Angela De Bonis , Italy
Abílio De Jesus , Portugal
José António Fonseca De Oliveira
Correia , Portugal
Ismail Demir , Turkey
Luigi Di Benedetto , Italy
Maria Laura Di Lorenzo, Italy
Marisa Di Sabatino, Norway
Luigi Di Sarno, Italy
Ana María Díez-Pascual , Spain
Guru P. Dinda , USA
Hongbiao Dong, China
Mingdong Dong , Denmark
Frederic Dumur , France
Stanislaw Dymek, Poland
Kaveh Edalati , Japan
Philip Eisenlohr , USA
Luis Evangelista , Norway
Michele Fedel , Italy
Francisco Javier Fernández Fernández ,
Spain
Isabel J. Ferrer , Spain
Massimo Fresta, Italy
Samia Gad , Egypt
Pasquale Gallo , Finland
Sharanabasava Ganachari, India
Santiago Garcia-Granda , Spain
Carlos Garcia-Mateo , Spain

Achraf Ghorbal , Tunisia
Georgios I. Giannopoulos , Greece
Ivan Giorgio , Italy
Andrea Grilli , Italy
Vincenzo Guarino , Italy
Daniel Guay, Canada
Jenő Gubicza , Hungary
Xuchun Gui , China
Benoit Guiffard , France
Zhixing Guo, China
Ivan Gutierrez-Urrutia , Japan
Weiwei Han , Republic of Korea
Simo-Pekka Hannula, Finland
A. M. Hassan , Egypt
Akbar Heidarzadeh, Iran
Yi Huang , United Kingdom
Joshua Ighalo, Nigeria
Saliha Ilican , Turkey
Md Mainul Islam , Australia
Ilia Ivanov , USA
Jijo James , India
Hafsa Jamshaid , Pakistan
Hom Kandel , USA
Kenji Kaneko, Japan
Rajesh Kannan A , Democratic People's
Republic of Korea
Mehran Khan , Hong Kong
Akihiko Kimura, Japan
Ling B. Kong , Singapore
Pramod Koshy, Australia
Hongchao Kou , China
Alexander Kromka, Czech Republic
Abhinay Kumar, India
Avvaru Praveen Kumar , Ethiopia
Sachin Kumar, India
Paweł Kłosowski , Poland
Wing-Fu Lai , Hong Kong
Luciano Lamberti, Italy
Fulvio Lavecchia , Italy
Laurent Lebrun , France
Joon-Hyung Lee , Republic of Korea
Cristina Leonelli, Italy
Chenggao Li , China
Rongrong Li , China
Yuanshi Li, Canada

Guang-xing Liang , China
Barbara Liguori , Italy
Jun Liu , China
Yunqi Liu, China
Rong Lu, China
Zhiping Luo , USA
Fernando Lusquiños , Spain
Himadri Majumder , India
Dimitrios E. Manolakos , Greece
Necmettin Maraşlı , Turkey
Alessandro Martucci , Italy
Roshan Mayadunne , Australia
Mamoun Medraj , Canada
Shazim A. Memon , Kazakhstan
Pratima Meshram , India
Mohsen Mhadhbi , Tunisia
Philippe Miele, France
Andrey E. Miroshnichenko, Australia
Ajay Kumar Mishra , South Africa
Hossein Moayedi , Vietnam
Dhanesh G. Mohan , United Kingdom
Sakar Mohan , India
Namdev More, USA
Tahir Muhmood , China
Faisal Mukhtar , Pakistan
Dr. Tauseef Munawar , Pakistan
Roger Narayan , USA
Saleem Nasir , Pakistan
Elango Natarajan, Malaysia
Rufino M. Navarro, Spain
Miguel Navarro-Cia , United Kingdom
Behzad Nematollahi , Australia
Peter Niemz, Switzerland
Hiroschi Noguchi, Japan
Dariusz Oleszak , Poland
Laurent Orgéas , France
Togay Ozbakkaloglu, United Kingdom
Marián Palcut , Slovakia
Davide Palumbo , Italy
Gianfranco Palumbo , Italy
Murlidhar Patel, India
Zbyšek Pavlík , Czech Republic
Alessandro Pegoretti , Italy
Gianluca Percoco , Italy
Andrea Petrella, Italy

Claudio Pettinari , Italy
Giorgio Pia , Italy
Candido Fabrizio Pirri, Italy
Marinos Pitsikalis , Greece
Alain Portavoce , France
Simon C. Potter, Canada
Ulrich Prah, Germany
Veena Ragupathi , India
Kawaljit Singh Randhawa , India
Baskaran Rangasamy , Zambia
Paulo Reis , Portugal
Hilda E. Reynel-Avila , Mexico
Yuri Ribakov , Israel
Aniello Riccio , Italy
Anna Richelli , Italy
Antonio Riveiro , Spain
Marco Rossi , Italy
Fernando Rubio-Marcos , Spain
Francesco Ruffino , Italy
Giuseppe Ruta , Italy
Sachin Salunkhe , India
P Sangeetha , India
Carlo Santulli, Italy
Fabrizio Sarasini , Italy
Senthil Kumaran Selvaraj , India
Raffaele Sepe , Italy
Aabid H Shalla, India
Poorva Sharma , China
Mercedes Solla, Spain
Tushar Sonar , Russia
Donato Sorgente , Italy
Charles C. Sorrell , Australia
Damien Soulat , France
Adolfo Speghini , Italy
Antonino Squillace , Italy
Koichi Sugimoto, Japan
Jirapornchai Suksaeree , Thailand
Baozhong Sun, China
Sam-Shajing Sun , USA
Xiaolong Sun, China
Yongding Tian , China
Hao Tong, China
Achim Trampert, Germany
Tomasz Trzepieciński , Poland
Kavimani V , India




Matjaz Valant , Slovenia
Mostafa Vamegh, Iran
Lijing Wang , Australia
Jörg M. K. Wiezorek , USA
Guosong Wu, China
Junhui Xiao , China
Guoqiang Xie , China
YASHPAL YASHPAL, India
Anil Singh Yadav , India
Yee-wen Yen, Taiwan
Hao Yi , China
Wenbin Yi, China
Tetsu Yonezawa, Japan
Hiroshi Yoshihara , Japan
Bin Yu , China
Rahadian Zainul , Indonesia
Lenka Zaji#c#kova# , Czech Republic
Zhigang Zang , China
Michele Zappalorto , Italy
Gang Zhang, Singapore
Jinghuai Zhang, China
Zengping Zhang, China
You Zhou , Japan
Robert Černý , Czech Republic

Contents



Hybrid Effect of Wollastonite Fiber and Carbon Fiber on the Mechanical Properties of Oil Well Cement Pastes

Jianglin Zhu , Jiangxiong Wei, Qijun Yu, Mingbiao Xu, and Yuwei Luo
Research Article (9 pages), Article ID 4618035, Volume 2020 (2020)

Effective Absorption Capacity Examined by Isothermal Calorimetry: Effect of Pore Structure and Water-to-Cement Ratio

Joo-Ha Lee , Do Guen Yoo , and Bo Yeon Lee 
Research Article (8 pages), Article ID 7692751, Volume 2020 (2020)

Influence of the Amount of Steel Fibers on Fracture Energy and Drying Shrinkage of HPRCC

Weina Guo , Peng Zhang , Yupeng Tian, Bing Wang, and Wan Ma
Research Article (15 pages), Article ID 8459145, Volume 2020 (2020)

Research Article

Hybrid Effect of Wollastonite Fiber and Carbon Fiber on the Mechanical Properties of Oil Well Cement Pastes

Jianglin Zhu ^{1,2}, Jiangxiong Wei,¹ Qijun Yu,¹ Mingbiao Xu,³ and Yuwei Luo⁴

¹School of Materials Science and Engineering, South China University of Technology, Guangzhou 510000, China

²Southern Marine Science and Engineering Guangdong Laboratory (Zhanjiang), Zhanjiang 524000, China

³School of Petroleum Engineering, Yangtze University, Wuhan 430000, China

⁴China Oilfield Services Limited Oilfield Chemicals Division, Beijing 100000, China

Correspondence should be addressed to Jianglin Zhu; jianglinzhu123@163.com

Received 30 April 2020; Revised 6 October 2020; Accepted 20 October 2020; Published 17 November 2020

Academic Editor: Rishi Gupta

Copyright © 2020 Jianglin Zhu et al. This is an open access article distributed under the Creative Commons Attribution License, which permits unrestricted use, distribution, and reproduction in any medium, provided the original work is properly cited.

Oil well cement is a type of natural brittle material that cannot be used directly in cementing operations. Fiber is a type of material that can effectively improve the strength and toughness of cement stone, and hybrid fiber materials can more effectively improve the performance of a cement sample. To overcome the natural defects of oil well cement, the new mineral fiber, i.e., wollastonite fiber, and common carbon fiber were used in oil well cement, and the micromorphology, mechanical properties, and stress-strain behavior of the cement were evaluated. The experimental results show that carbon fiber and wollastonite fiber are randomly distributed in the cement paste. The mechanical properties of the cement paste are improved by bridging and pulling out. The compressive strength, flexural strength, and impact strength of cement stone containing only carbon fiber or wollastonite fiber are higher than those of the pure cement, but too many fibers are not conducive to the development of mechanical properties. A mixture of 0.3% carbon fiber with 6% wollastonite fiber in oil well cement slurry results in a greater increase in compressive strength, flexural strength, and impact strength. In addition, compared with blank cement stone, the strain of the mixed cement stone increases substantially, and the elastic modulus decreases by 37.8%. The experimental results supply technical support for the design of a high-performance cement slurry system.

1. Introduction

The cementing operation injects cement slurry into the casing and formation annulus and forms a cement sheath after the cement slurry solidifies to effectively seal the layers and support and protect the casing [1]. After cementing, the cement sheath is subjected to impact force via various operations in the subsequent pressure testing, perforation, fracturing, and other construction processes, which require cement stone with good mechanical properties. Oil well cement is a type of brittle material that has poor resistance to external force [2]. Addition of reinforcement and toughening materials to cement can overcome the defects of oil well cement.

Currently, the main fibers used in oil well cement include polymer fibers and mineral fibers. Ahmed et al. [3] evaluated

the function of polypropylene fiber and found that the effect of polypropylene fiber on the density, rheology, and free liquid of cement slurry can be ignored, the compressive strength of cement stone is improved, and the permeability of cement stone is reduced. Iremonger et al. [4] applied reinforced fiber as a cement additive in a thermal recovery well. The reinforced fiber had a certain stabilizing effect on the compressive strength and Young's modulus of the cement sample under high temperature. Liu et al. [5] studied the effect of cellulose fiber on the properties of low-density cement paste. Mechanical properties such as the tensile strength and flexural strength of cement stone and the elastic deformation ability of cement stone were improved. Research results from Bu et al. [6] and Li et al. [7] showed that carbon fiber can effectively improve the mechanical properties and deformation ability of cement paste. These studies

demonstrated that the polymer fiber can improve the mechanical properties of the cement sheath, including compressive strength, impact strength, and crack phenomena during perforation.

In addition, Li et al. [8] and Li and Zhuang [9] studied the influence of brucite fiber on the performance of oil well cement. The results showed that the splitting tensile strength, compressive strength, and flexural strength of brucite fiber cement stone are much higher than those of pure cement stone, and the elastic modulus is decreased. Paivaa et al. [10], Jiang et al. [11], and Rambo et al. [12] showed that basalt fiber can improve the tensile strength, flexural strength, and other mechanical properties of cement paste. Kurata and Umemoto [13] studied the effect of aluminum borate whiskers on the performance improvement of polycarboxylic cement-based materials. The tensile strength of cement paste containing aluminum borate whiskers is three times that of the sample without whiskers, and the compressive strength increases. These studies demonstrate that materials with both micropowder and fiber properties show improved mechanical properties in cement-based materials.

Wollastonite fiber is a new type of mineral fiber that has not previously been used in oil well cement. This material is a chain-like metasilicate mineral with a special crystal structure and has the characteristics of mineral powder and fiber. Carbon fiber is one of the most commonly used strengthening and toughening materials in cement slurry. Certain reports have studied the hybrid effect of polymer fiber and inorganic mineral fiber and found that hybrid use of the two fibers can fully leverage the role of the fiber and more effectively improve the performance of cement stone [14]. Therefore, this work studies the effect of wollastonite fiber and carbon fiber in oil well cement and mixes them to study the mechanical properties of the hybrid fiber cement, thus supplying technical support for the design of a high-performance cementing slurry system.

2. Experimental Materials and Methods

2.1. Materials. API standard class G oil well cement was purchased from Gezhouba Special Cement Co., Ltd., China. The chemical composition of oil well cement is presented in Table 1. Wollastonite fiber and carbon fiber were commercially obtained from the market. The properties of wollastonite fiber are shown in Tables 2 and 3. The properties of carbon fiber are presented in Table 4. Filtrate reducer, enhancer, retarder, and dispersant were also sourced on the market from professional companies. These four materials are necessary additives for cement slurry and are used to reduce the water loss, improve the compressive strength, adjust the thickening time, and improve the fluidity of the cement slurry.

2.2. Preparation of Cement Slurry

2.2.1. Application Method of Carbon Fiber. Selected studies have shown that carbon fiber is easily agglomerated in the process of application and is not evenly dispersed in the

TABLE 1: Chemical composition of oil well cement.

CaO (%)	SiO ₂ (%)	Al ₂ O ₃ (%)	Fe ₂ O ₃ (%)	MgO (%)	SO ₃ (%)	Na ₂ O + K ₂ O (%)
64.6	22.2	3.7	4.8	1.3	2.9	0.5

TABLE 2: Basic properties of wollastonite fiber.

Average grain size (μm)	Aspect ratio	Density (g/cm^3)	Ignition loss (%)	Melting point ($^{\circ}\text{C}$)	Mohs hardness
48	>12	2.8	1.8	1540	4.5-5.5

cement slurry [15, 16]. Therefore, carbon fiber should be predispersed in the process of application. After weighing the prepared aqueous solution, carbon fiber of a specified quality is uniformly added to the aqueous solution, and the carbon fiber dispersion is formed after stirring via a corrugated agitator for approximately 30 s. The carbon fiber dispersion solution is used as the slurry preparation solution to prepare the cement slurry.

2.2.2. Preparation of Cement Slurry. The cement slurries are prepared according to Table 5. The cement, filtrate reducer, enhancer, and dispersant of specified quality are weighed as dry powder, and water and retardant of a specified quality are weighed as mixing water. The use of carbon fiber refers to the steps described above, and wollastonite fiber is used as a component of dry powder. The materials are poured with the mixed water into the mixing cup and stirred at 4000 ± 200 r/min with a constant speed mixer (TG-3060A, Shenyang Taige Petroleum Instrument & Equipment Co., Ltd.), and the dry powder is added evenly within 15 s. After all of the mixed dry powder is poured into the mixing water, the mixing cup is covered, and stirring is continued for $35 \text{ s} \pm 1 \text{ s}$. In this manner, the cement slurry system is prepared.

2.3. Mechanical Properties Test. After the cement slurry is prepared, it is poured into the compressive strength, flexural strength, and impact strength test molds and cured in a water bath at 80°C and atmospheric pressure. The sample sizes of the compressive strength and flexural strength test samples are $50.8 \text{ mm} \times 50.8 \text{ mm} \times 50.8 \text{ mm}$ and $40 \text{ mm} \times 40 \text{ mm} \times 160 \text{ mm}$, respectively. The compressive strength and flexural strength of cement stone are tested by a fully automatic flexural and compression testing machine (YAW-300C, Ji'nan Zhongluchang Testing Machine Manufacturing Co., Ltd., China). The compressive strength test uses a constant speed compressive stress of $72 \text{ kN}/\text{min}$ according to the Chinese standard GB/T 19139-2012. The flexural strength is tested by the three-point bending method. The sample size for the impact strength test is $10 \text{ mm} \times 15 \text{ mm} \times 120 \text{ mm}$. The impact strength of the cement samples is tested by a pendulum impact tester (XJY-50, Chengdeshi Shipeng Detection Equipment Co., Ltd., China).

TABLE 3: Chemical composition of wollastonite fiber.

SiO ₂ (%)	CaO (%)	Al ₂ O ₃ (%)	MgO (%)	Fe ₂ O ₃ (%)	Others (%)
51.5	42.4	2.1	0.7	0.5	2.8

TABLE 4: Basic properties of carbon fiber.

Length (mm)	Single diameter (μm)	Tensile strength (MPa)	Tensile modulus (GPa)	Density (g/cm^3)	Elongation (%)	Carbon content (%)
1	7	3530	230	1.78	1.5	≥ 96

TABLE 5: Mix compositions of oil-well cement slurries.

Sample number	Cement (wt.%)	Water (wt. %)	Filtrate reducer (wt. %)	Enhancer (wt. %)	Dispersant (wt. %)	Retarder (wt. %)	Carbon fiber (wt. %)	Wollastonite fiber (wt. %)
P	100	44	2	1.5	0.8	0.5	0	0
C1	100	44	2	1.5	0.8	0.5	0.1	0
C2	100	44	2	1.5	0.8	0.5	0.2	0
C3	100	44	2	1.5	0.8	0.5	0.3	0
C4	100	44	2	1.5	0.8	0.5	0.4	0
W1	100	44	2	1.5	0.8	0.5	0	2
W2	100	44	2	1.5	0.8	0.5	0	4
W3	100	44	2	1.5	0.8	0.5	0	6
W4	100	44	2	1.5	0.8	0.5	0	8
CW1	100	44	2	1.5	0.8	0.5	0.3	3
CW2	100	44	2	1.5	0.8	0.5	0.15	6
CW3	100	44	2	1.5	0.8	0.5	0.3	6

2.4. Test of Stress-Strain Behavior. The test sample was prepared according to the preparation process of cement slurry mechanical property test sample. After 28-day curing, a universal testing machine (HY-20080, Shanghai Hengyi Precision Instrument Co., Ltd., China) was used to test the unconfined stress-strain of cement stone according to the Chinese standard GB/T 50266-2013.

2.5. Fracture Surface Morphology Observation of Cement Sample. The cement paste sample was crushed, and the regular thin section on the middle part was selected to stop hydration treatment. The samples were dried at constant temperature in the oven. After the samples were cooled, they were pasted on the test bench. The samples were observed by the scanning electron microscope (SU 8010, Hitachi).

3. Results and Discussion

3.1. Mechanism of Fiber-Reinforced Cement Paste. Fiber is a type of material with a high aspect ratio. The microstructure of the two types of fiber materials was observed via SEM. Figures 1(a) and 1(b) show SEM images of single carbon fiber and wollastonite fiber, respectively. As observed from Figure 1(a), the carbon fiber is longer, the length diameter ratio is larger, and the shape is more regular. The length diameter ratio of the wollastonite fiber is small, and the length is short, as shown in Figure 1(b).

Figure 2 shows SEM images of cement stone with 0.3% carbon fiber. It can be observed from Figure 2(a) that the

distribution of carbon fiber in the cement paste is disorderly and without clusters. Figure 2(b) shows the “pull-out” and “bridging” effect of carbon fiber in the cement paste. Because carbon fiber has a high aspect ratio, when cracks appear in the carbon fiber cement stone specimen, the fiber transmits the tensile stress to the matrix through the cohesive force and mechanical bite force, which limits the expansion of local cracks in the cement specimen. When the development of cracks is inevitable, the fibers in the cracks are stretched, pulled out or broken. At this time, a large amount of energy is consumed, and thus the fracture toughness of cement materials can be greatly improved, and the brittleness of the matrix during the fracture can be significantly reduced [17–19]. In the area where the distribution of carbon fiber is consistent with the direction of crack development, the crack is difficult to deflect and can only continue to expand along the original direction. At this time, the carbon fiber close to the crack tip is not pulled out or broken but forms a similar “bridging” function on both sides of the crack and produces a compressive stress on the crack surface, which offsets the external stress to a certain extent, thus preventing crack growth and enhancing the mechanical properties of the cement paste [20].

Figure 3 shows the fracture morphology of wollastonite fiber cement stone. It can be observed in Figure 3(a) that wollastonite fibers are randomly distributed inside the cement stone and cross-linked with the cement stone matrix. Figure 3(b) shows the structure of carbon fiber interpenetrating with the cement hydration products in the cement matrix. Wollastonite fiber plays a similar role as carbon

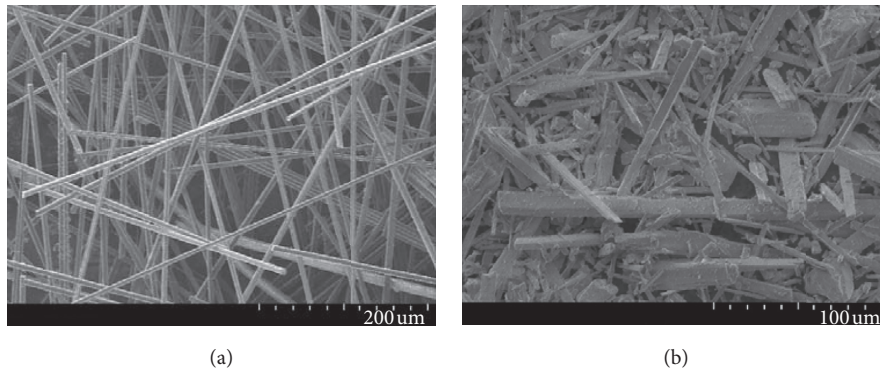


FIGURE 1: Morphology of single carbon fiber and wollastonite fiber. (a) Carbon fiber. (b) Wollastonite fiber.

fiber in the cement paste. Via the “bridging” and “pulling out” functions, the toughness and strength of the cement paste are improved.

3.2. Mechanical Properties of Cement Slurry

3.2.1. Effect of Carbon Fiber on the Mechanical Properties of Cement Paste. The main mechanical properties of the cement slurry include compressive strength, flexural strength, and impact strength. The compressive strength of cement stone represents the ability to maintain the integrity of the cement stone under compressive stress and is the maximum stress of cement stone under the action of a uniform compressive stress on the unit stress contact surface [21]. The flexural strength can be directly used to characterize the ability of the cement sheath to bear external shear and indirectly used to characterize the toughness of cement stone [22]. The impact strength is the energy consumed by the cement specimen after impact fracture, which indicates the ability of the cement stone to withstand impact. The impact strength is a significant index in evaluation of the toughness of cement stone, and its value can directly reflect the toughness and quantitatively characterize the toughening effect of the cement stone [23].

The compressive strength, flexural strength, and impact strength of cement pastes with different amounts of carbon fiber were evaluated under the conditions of temperature curing for 1 d, 3 d, 7 d, 14 d, and 28 d, and the results are presented in Figures 4–6. It can be observed from the figures that with the extension of curing time, the compressive strength, flexural strength, and impact strength of cement stone are increased.

As shown in Figure 4, as the fiber content increases, the compressive strength of the cement paste increases. The compressive strengths of cement paste containing 0.1%, 0.2%, 0.3%, and 0.4% carbon fiber are increased by 8%, 11.25%, 17.5%, and 19.75%, respectively, compared with those of pure cement paste. The addition of carbon fiber can improve the compressive strength of cement paste.

The results in Figure 5 show that the flexural strengths of cement paste with different carbon fiber content vary significantly. Carbon fiber can improve the flexural strength of cement paste, but too much carbon fiber has a negative

impact on the flexural strength. If the content of carbon fiber is greater than 0.3%, the flexural strength decreases. If the curing time is 1 day, the flexural strengths of cement stone containing 0.1%, 0.2%, 0.3%, and 0.4% carbon fiber are 4.7%, 12.7%, 25.4%, and 15.9% higher, respectively, than that of pure cement stone. With the extension of curing time, the flexural strength is increased. When the curing time reaches 28 days, the flexural strength of cement stone containing 0.3% carbon fiber is the largest and is 30.3% higher than that of the pure cement stone, reaching 12.9 MPa.

Figure 6 shows that carbon fiber can effectively improve the toughness of cement, but excessive carbon fiber is not conducive to the development of impact strength. When the curing time is 1 day, the impact strength of cement stone containing 0.3% carbon fiber is the largest, reaching 1.8 kJ/m². With the increase of curing time, the impact strength increases. When the curing time is 28 days, the flexural strengths of cement stone containing 0.1%, 0.2%, 0.3%, and 0.4% carbon fiber are 7.5%, 14%, 18.3%, and 12.9% higher, respectively, than those of pure cement stone. Carbon fiber can effectively improve the impact strength of cement paste.

3.2.2. Effect of Wollastonite Fiber on the Mechanical Properties of Cement Slurry. The compressive strength, flexural strength, and impact strength of cement paste with different wollastonite fiber content were tested, and the test results are presented in Figures 7–9. The data in Figure 7 show that the compressive strength of cement stone increases with the extension of curing time. The compressive strength of 8% wollastonite fiber cement paste was 26.4% higher than that of the pure cement paste after curing for 1 day. After curing for 28 days, compared with the pure sample, the compressive strengths of cement stone increased by 5.6%, 10.3%, 17.8%, and 22% with the addition of 2%, 4%, 6%, and 8% wollastonite fiber, respectively. Wollastonite fiber can improve the compressive strength of cement paste and the ability of the cement sheath to resist external load.

Figure 8 shows the flexural strength evaluation results of wollastonite fiber cement samples. It can be observed from the evaluation results that wollastonite fiber can significantly improve the flexural strength of cement paste. With the increase in curing age, the flexural strength of cement stone is increased. When the wollastonite fiber content is 6%, the

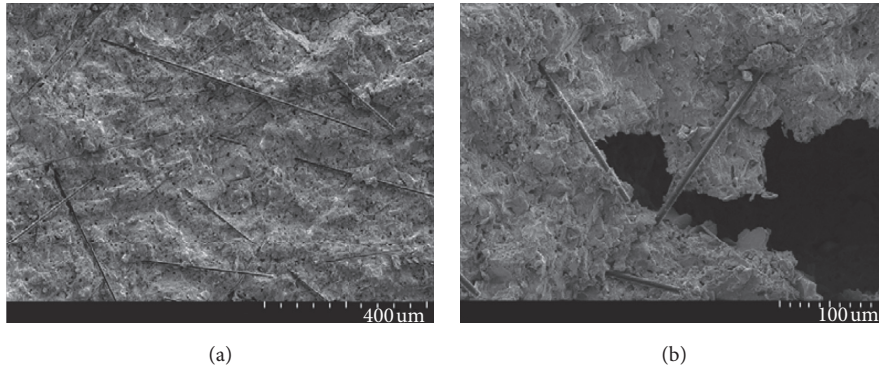


FIGURE 2: Fracture morphology of carbon fiber cement sample.

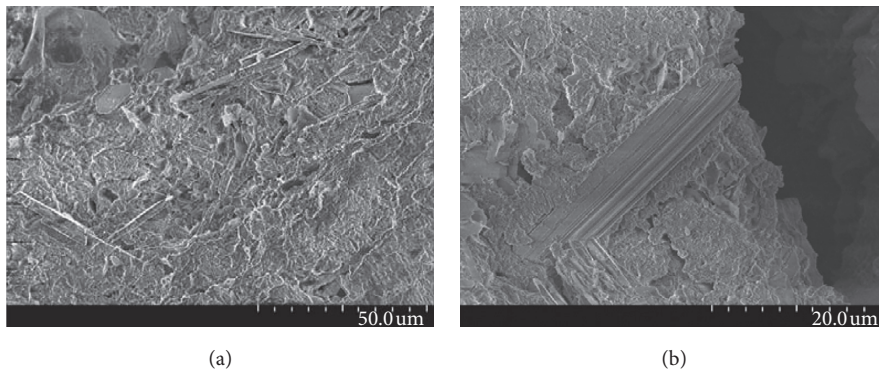


FIGURE 3: Fracture morphology of wollastonite fiber cement sample.

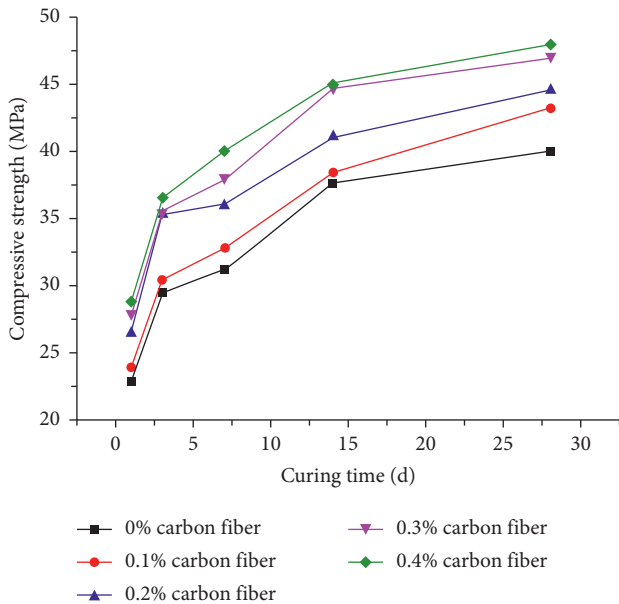


FIGURE 4: Compressive strength of carbon fiber cement stone.

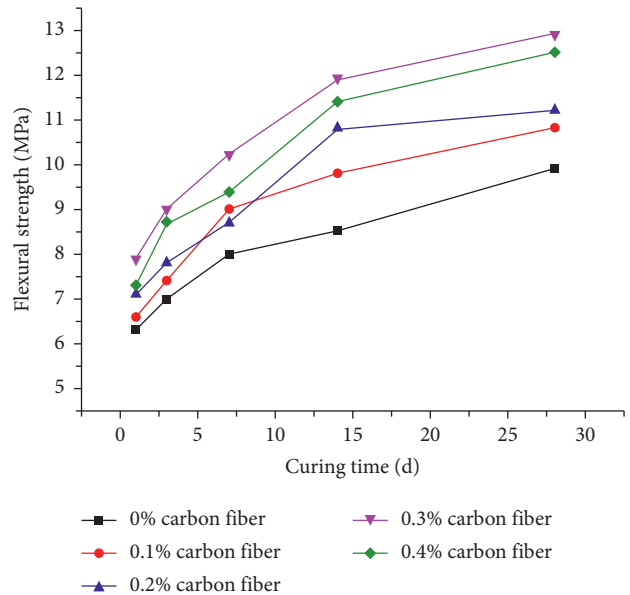


FIGURE 5: Flexural strength of carbon fiber cement paste.

flexural strength of the cement sample increases most obviously, by approximately 30.2% and 23.2% compared with the pure sample after curing for 1 day and 28 days, respectively.

Figure 9 shows the test results of the impact strength of wollastonite fiber cement stone at different curing ages. Wollastonite fiber can improve the impact strength of the

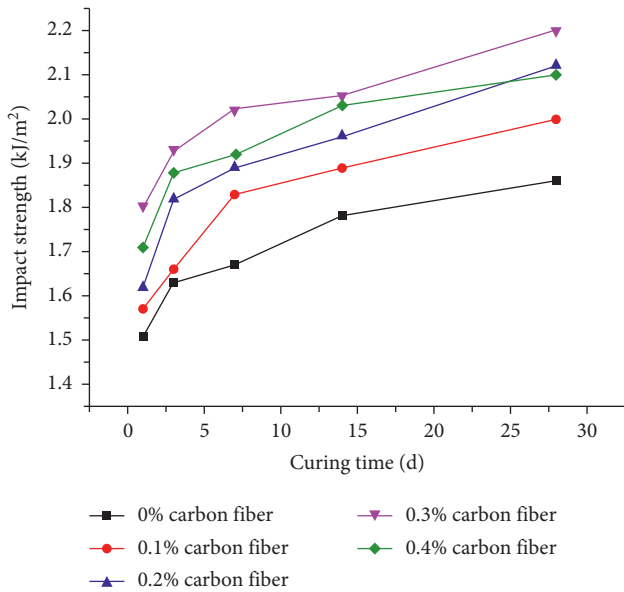


FIGURE 6: Impact strength of carbon fiber cement stone.

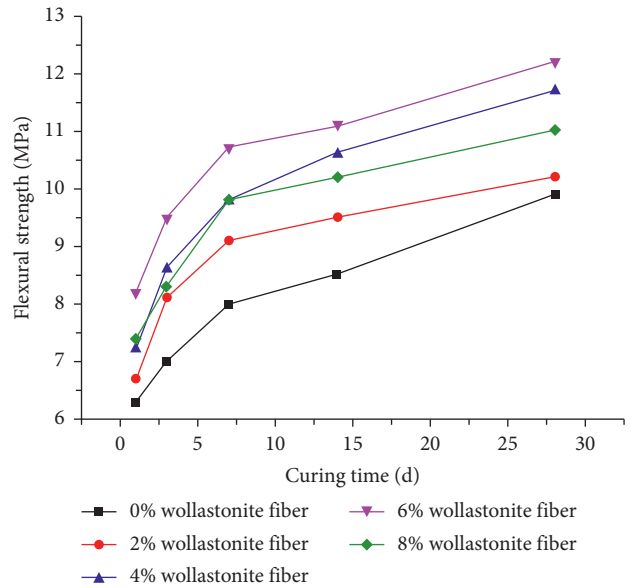


FIGURE 8: Flexural strength of wollastonite fiber cement stone.

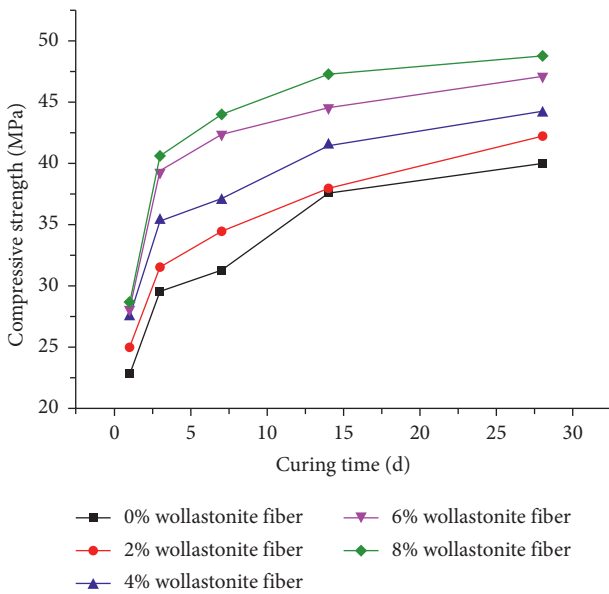


FIGURE 7: Compressive strength of wollastonite fiber cement stone.

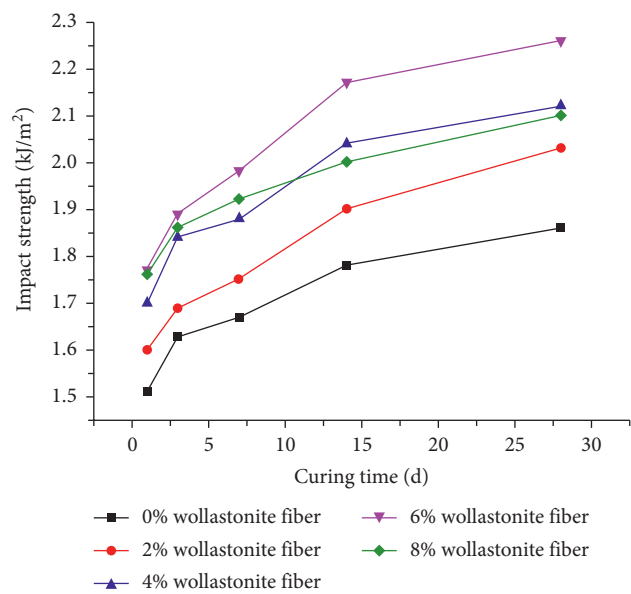


FIGURE 9: Impact strength of wollastonite fiber cement stone.

cement stone as well as the conventional fiber. Wollastonite fiber improves the crushing absorption energy of the cement stone. With the extension of curing age, the impact strength of the sample is increased. After curing for one day, the impact strength of the wollastonite fiber cement sample is 17.2% higher than that of the pure sample. After curing for 28 days, the impact strengths of 2%, 4%, 6%, and 8% wollastonite fiber increased by 9.1%, 14%, 21.5%, and 12.9%, respectively. The development of the impact strength of the cement sample is the best when the content of wollastonite fiber is 6%, but too much wollastonite fiber is not conducive to the development of the impact strength of the cement.

3.2.3. Synergistic Effect of Carbon Fiber and Wollastonite Fiber on the Mechanical Properties of Cement Paste.

From the evaluation of the mechanical properties of carbon fiber cement stone and wollastonite fiber cement stone, it was found that when the amount of carbon fiber is greater than 0.3% or that of wollastonite fiber is greater than 6%, the flexural strength and impact strength of the cement stone might decrease. Therefore, in this experiment, three proportions of hybrid fiber, namely, 0.3% carbon fiber and 3% wollastonite fiber (CW1), 0.15% carbon fiber and 6% wollastonite fiber (CW2), and 0.3% carbon fiber and 6% wollastonite fiber (CW3), were mixed with cement, and the performances of the hybrid fiber cement slurry were evaluated. The performance of the 0.3% carbon fiber (C3), 6%

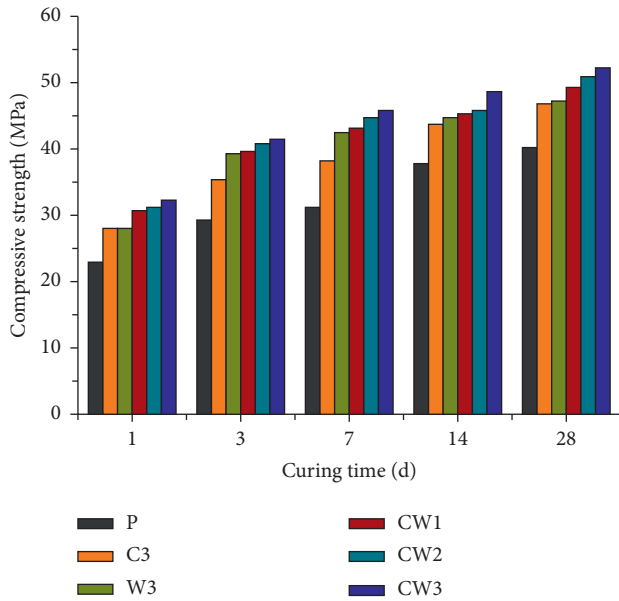


FIGURE 10: Compressive strength of cement stone mixed with carbon fiber and wollastonite fiber.

wollastonite fiber cement sample (W3), and pure cement stone (P) were compared, and the experimental results are presented in Figures 10–12.

It can be observed from the experimental results that in different curing stages, both fibers can significantly improve the mechanical properties of cement stone, and the compressive strength, flexural strength, and impact strength of the hybrid fiber cement stone are higher than those of single fiber cement stone. Figure 10 shows that the compressive strengths of the three proportions of mixed fiber cement slurry are higher than those of the single fiber cement slurry. When the curing time is 28 d, the compressive strengths of samples CW1, CW2, and CW3 are increased by 23%, 26.8%, and 30.8%, respectively, compared with those of the pure cement slurry. The optimal addition amount of single fiber can still greatly improve the effect after mixing. Figure 11 shows a comparison of flexural strength. Fiber contributes substantially to the flexural strength of cement, and hybrid fiber has a better effect. When the curing time is 28 days, the flexural strength of the CW3 sample is 10.4%, 13.1%, and 39.4% higher than that of carbon fiber sample, wollastonite fiber sample, and pure cement, respectively. Figure 12 shows that the impact strength of the mixed fiber cement slurry is higher than that of the single fiber. The impact strengths of the CW1, CW2, and CW3 samples are 24.2%, 25.3%, and 29% higher than those of the pure cement slurry, respectively. The experimental results show that the mixed fiber can improve the cement slurry better than the single fiber, and the optimal additive combination of fibers can also achieve better performance.

3.3. *Stress-Strain Behavior of Cement Paste.* Figure 13 presents the stress-strain behavior of pure cement stone (P), carbon fiber

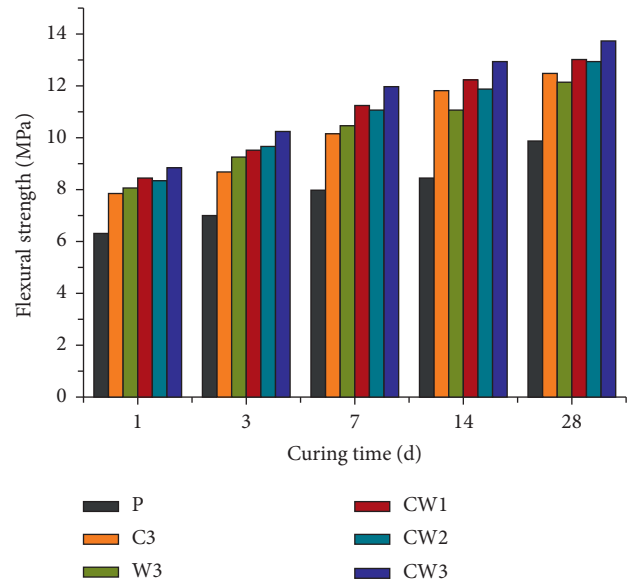


FIGURE 11: Flexural strength of cement stone mixed with carbon fiber and wollastonite fiber.

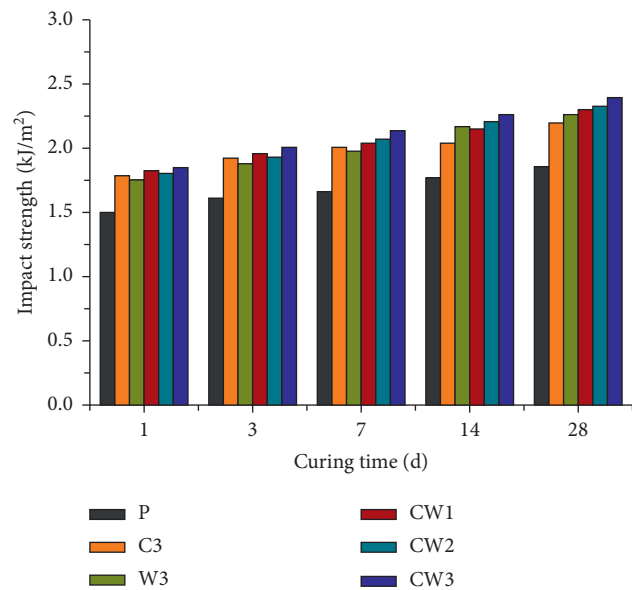


FIGURE 12: Impact strength of cement stone mixed with carbon fiber and wollastonite fiber.

cement stone (C3), wollastonite fiber cement stone (W3), and cement stone mixed with two fibers (CW) under a compression load. It can be observed from the stress-strain curve that the stress-strain curve of pure cement paste is approximately a straight line. When the pure cement is subjected to stress compression, it displays brittleness, and when it reaches the maximum stress, the cement is rapidly destroyed. When the cement stone with fiber material is compressed, a straight line appears at first. With continuous loading, a nonlinear curve appears, and creep occurs continuously, showing elastic deformation ability [24, 25]. The stress of the cement paste is increased and the strain of the cement paste is also increased by

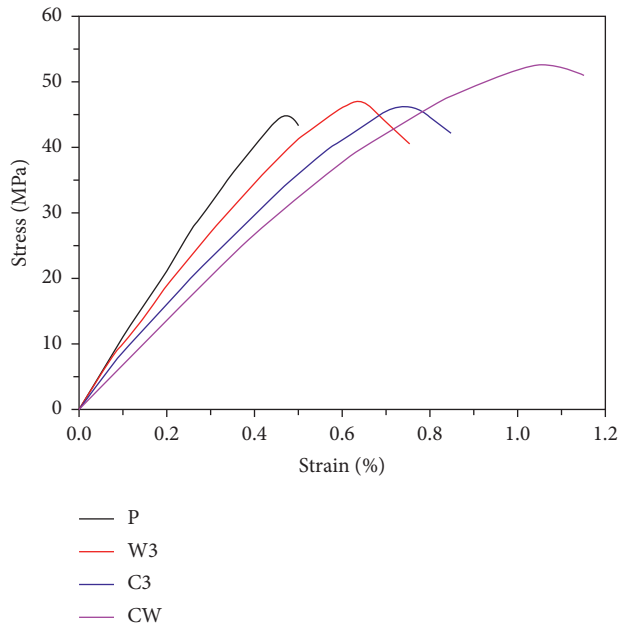


FIGURE 13: Stress-strain curve of fiber cement paste.

the single fiber. Under the same stress condition, the strain of cement stone is the largest when the two fibers are mixed, followed by that of the carbon fiber cement stone. The deformation ability of fiber cement is strong, and the use of mixed materials can improve the load resistance of cement. The elastic model of cement paste can be calculated from the stress-strain curve. The experimental results demonstrate that the strain of blank cement is 0.4%, and the elastic modulus is 9.8 GPa. Compared with the pure cement stone, the strain of the mixed cement stone increases substantially, and the elastic modulus decreases by 37.8%. The experimental results show that the hybrid effect of carbon fiber and wollastonite fiber can improve the deformation ability and elasticity of cement paste.

4. Conclusion

- (1) Carbon fiber and wollastonite fiber are scattered in the cement slurry, and the mechanical properties of the cement paste are improved by bridging and pulling out behaviors.
- (2) Single carbon fiber or wollastonite fiber can improve the compressive strength, flexural strength, and impact strength of cement paste, but too many fibers are not conducive to the development of flexural strength and impact strength of cement paste.
- (3) The mechanical properties of cement stone can be enhanced by mixing two types of fibers. The flexural strength, compressive strength, and impact strength of hybrid fiber cement stone are higher than those of single fiber cement stone.
- (4) The stress-strain behavior shows that the hybrid fiber cement stone has the highest stress and the largest strain. The elastic modulus decreases substantially,

and the deformation ability of the cement stone increases greatly.

Data Availability

The data used to support the findings of this study are included within the article.

Conflicts of Interest

The authors declare that they have no conflicts of interest regarding the publication of this paper.

Acknowledgments

This work was supported by the National Science and Technology Major Project (no. 2016ZX05026-002) funded by the Chinese Government.

References

- [1] N. Jafariefad, M. R. Geiker, Y. Gong, P. Skalle, Z. Zhang, and J. He, "Cement sheath modification using nanomaterials for long-term zonal isolation of oil wells: Review," *Journal of Petroleum Science and Engineering*, vol. 156, pp. 662–672, 2017.
- [2] J. Song, M. Xu, W. Liu, X. Wang, and Y. Wu, "Synergistic effect of latex powder and rubber on the properties of oil well cement-based composites," *Advances in Materials Science and Engineering*, vol. 2018, Article ID 4843816, 9 pages, 2018.
- [3] A. Ahmed, S. Elkhatatny, R. Gajbhiye et al., "Effect of polypropylene fibers on oil-well cement properties at HPHT condition," in *Proceedings of the SPE Kingdom of Saudi Arabia Annual Technical Symposium and Exhibition*, Dammam, Saudi Arabia, April 2018.
- [4] S. S. Iremonger, M. Bolt, and S. C. Lawrence, "Enhanced thermal well integrity through the use of a new cement tensile strength-enhancing fiber," in *Proceedings of the SPE Canada Heavy Oil Technical Conference*, Calgary, Canada, June 2015.
- [5] K. Liu, X. Cheng, X. Zhang, X. Guo, and J. Zhuang, "Design of low-density cement optimized by cellulose-based fibre for oil and natural gas wells," *Powder Technology*, vol. 338, pp. 506–518, 2018.
- [6] Y. H. Bu, R. H. Wang, and R. C. Cheng, "Performance of fiber cement slurry for well cementation," *Oil Drilling and Production Technology*, vol. 27, no. 2, pp. 25–27, 2005.
- [7] M. Li, Y. J. Yang, and X. Y. Guo, "Mechanical properties of carbon fiber reinforced oil well cement composites," *Fuhe Cailiao Xuebao/Acta Materialiae Compositae Sinica*, vol. 32, no. 3, pp. 782–788, 2015.
- [8] M. Li, Y. J. Yang, J. Z. Jin et al., "Reinforced mechanical properties and mechanism of well-cementing stones by brucite fiber," *Natural Gas Industry*, vol. 35, no. 6, pp. 82–86, 2015.
- [9] X. K. Li and J. Zhuang, "Performance research of brucite fibers reinforced oil well cement paste," *Oilfield Chemistry*, vol. 32, no. 2, pp. 169–174, 2015.
- [10] L. C. M. Paiva, I. M. Ferreira, A. E. Martinelli, J. C. d. O. Freitas, and U. T. Bezerra, "Milled basalt fiber reinforced Portland slurries for oil well applications," *Journal of Petroleum Science and Engineering*, vol. 175, pp. 184–189, 2019.

- [11] C. Jiang, K. Fan, F. Wu, and D. Chen, "Experimental study on the mechanical properties and microstructure of chopped basalt fibre reinforced concrete," *Materials & Design*, vol. 58, no. 6, pp. 187–193, 2014.
- [12] D. A. S. Rambo, F. D. A. Silva, R. D. T. Filho et al., "Tensile strength of a calcium-aluminate cementitious composite reinforced with basalt textile in a high-temperature environment," *Cement & Concrete Composites*, vol. 70, pp. 183–193, 2016.
- [13] S. Kurata and K. Umemoto, "Study on the mechanical properties of polycarboxylate cement containing aluminoborate whisker," *Journal of the Japanese Society for Dental Materials & Devices*, vol. 25, pp. 246–250, 2006.
- [14] M. Li, Y. Yang, M. Liu, X. Guo, and S. Zhou, "Hybrid effect of calcium carbonate whisker and carbon fiber on the mechanical properties and microstructure of oil well cement," *Construction and Building Materials*, vol. 93, no. 1, pp. 995–1002, 2015.
- [15] V. J. Ferrari, J. B. de Hanai, and R. A. de Souza, "Flexural strengthening of reinforcement concrete beams using high performance fiber reinforcement cement-based composite (HPRCC) and carbon fiber reinforced polymers (CFRP)," *Construction and Building Materials*, vol. 48, no. 19, pp. 485–498, 2013.
- [16] Y. Xu and D. D. L. Chung, "Silane-treated carbon fiber for reinforcing cement," *Carbon*, vol. 39, no. 13, pp. 1995–2001, 2001.
- [17] S. Chakraborty, S. P. Kundu, A. Roy, B. Adhikari, and S. B. Majumder, "Effect of jute as fiber reinforcement controlling the hydration characteristics of cement matrix," *Industrial & Engineering Chemistry Research*, vol. 52, no. 3, pp. 1252–1260, 2013.
- [18] W. T. Lin, R. Huang, C. L. Lee et al., "Effect of steel fiber on the mechanical properties of cement-based composites containing silica fume," *Journal of Marine Science & Technology*, vol. 16, no. 3, pp. 214–221, 2008.
- [19] A. Peled, J. Jones, and S. P. Shah, "Effect of matrix modification on durability of glass fiber reinforced cement composites," *Materials and Structures*, vol. 38, no. 2, pp. 163–171, 2005.
- [20] E. M. Bezerra, A. P. Joaquim, H. Savastano Jr., V. M. John, and V. Agopyan, "The effect of different mineral additions and synthetic fiber contents on properties of cement based composites," *Cement and Concrete Composites*, vol. 28, no. 6, pp. 555–563, 2006.
- [21] J. Song, M. Xu, W. Liu et al., "Thermoplastic rubber (TPR) modified by a silane coupling agent and its influence on the mechanical properties of oil well cement pastes," *Advances in Materials Science and Engineering*, vol. 2019, Article ID 3587081, 11 pages, 2019.
- [22] P. Jamsawang, P. Voottipruex, and S. Horpibulsuk, "Flexural strength characteristics of compacted cement-polypropylene fiber sand," *Journal of Materials in Civil Engineering*, vol. 27, no. 9, Article ID 04014243, 2014.
- [23] V. Bindiganavile, N. Banthia, and B. Aarup, "Impact response of ultra-high-strength fiber-reinforced cement composite," *ACI Materials Journal*, vol. 99, no. 6, pp. 543–548, 2002.
- [24] A. Noushini, F. Aslani, A. Castel, R. I. Gilbert, B. Uy, and S. Foster, "Compressive stress-strain model for low-calcium fly ash-based geopolymer and heat-cured Portland cement concrete," *Cement and Concrete Composites*, vol. 73, pp. 136–146, 2016.
- [25] S. B. Zhao, M. S. Zhao, X. Y. Zhang et al., "Study on complete stress-strain curves of steel fiber reinforced lightweight aggregate concrete under uniaxial compression," *Journal of Building Structures*, vol. 40, no. 5, pp. 181–190, 2019.

Research Article

Effective Absorption Capacity Examined by Isothermal Calorimetry: Effect of Pore Structure and Water-to-Cement Ratio

Joo-Ha Lee ¹, Do Guen Yoo ¹, and Bo Yeon Lee ²

¹Department of Civil Engineering, The University of Suwon, Hwaseong-si 18323, Republic of Korea

²Department of Architectural Engineering, The University of Suwon, Hwaseong-si 18323, Republic of Korea

Correspondence should be addressed to Bo Yeon Lee; bylee@suwon.ac.kr

Received 23 April 2020; Accepted 5 June 2020; Published 24 June 2020

Guest Editor: Young H. Kim

Copyright © 2020 Joo-Ha Lee et al. This is an open access article distributed under the Creative Commons Attribution License, which permits unrestricted use, distribution, and reproduction in any medium, provided the original work is properly cited.

The accurate measurement of effective absorption capacity is crucial for highly absorptive materials when they are used within cement-based materials. In this study, a method for examining effective absorption capacity using isothermal calorimetry is reviewed and investigated in detail to accommodate different circumstances. Specifically, the effect of different pore structures and water-to-cement ratios in determining effective absorption capacity is experimentally examined using activated carbon fibre and powdered activated carbon. The results suggest that the method may be suitable for porous materials with micropores but not suitable for those with mesopores. Also, the results indicate that the effective absorption capacity value can change with the water-to-cement ratio used. These findings can be used to find the effective absorption capacity of highly absorptive materials more accurately using the isothermal calorimetry method.

1. Introduction

Cement-based materials such as concrete gain their strength through chemical reaction called hydration. Hydration occurs between cement and water, eventually forming hydration products or hardened cement paste. It is this hardened cement paste that gives concrete its major properties such as strength, porosity, shrinkage, and durability. When the water-to-cement ratio (w/c) is increased, strength tends to decrease, porosity and shrinkage increase, and overall durability tends to decrease. Thus, it is crucial that precise amount of water be used in concrete mix design in order to achieve expected properties.

For concrete that is used for general purposes, mix proportion design to reach a target w/c is not so challenging. However, special concretes have been developed and are being researched for specific purposes using various admixtures. When these admixtures are highly absorptive, modification to mix design should be performed; that is, water content should be increased in the amount that is absorbed by the material. Thus, absorption capacity of the material should be examined prior to carrying out mix design.

A good example of using highly absorptive material as an admixture to concrete is as an internal curing agent. The concept of internal curing of concrete emerged in the early 1990s [1] and has been consistently studied up until now. Internal curing is often referred to as “curing concrete from the inside out,” by providing additional curing water throughout the concrete mixture. For the curing agent, highly absorptive materials are used, which are expected to act as internal reservoirs that release water during the cement hydration process. For example, highly absorptive materials such as lightweight aggregate (LWA) [2–4], recycled concrete aggregate [5], superabsorbent polymers (SAPs) [6–8], or cellulose fibres [9, 10] are mixed into the concrete. These internal curing agents are known to improve cement hydration, increase strength, reduce early cracking, etc. [3, 11]. In addition, there is an evidence that highly absorptive fibres used for internal curing enhances early-age mechanical properties of cement-based materials. Jongvi-suttisun and Kurtis suggested that hardwood pulp fibres mitigate early-age cracking of mortar by increasing early tensile capacity, reducing modulus, and improving post-cracking toughness. These effects, combined with reductions

in autogenous shrinkage due to the effect of internal curing, lead to superior early-age crack mitigation than that achieved through the use of superabsorbent polymer [12]. This indicates that internal curing agents in the form of fibre could have mechanical advantages in addition to known effects of internal curing.

As water is a key factor of cement hydration, internal curing has been often applied to concrete that requires a low water-to-cement ratio (w/c) [3, 8, 13]. The low water content could be linked to self-desiccation, autogenous shrinkage, and incomplete cement hydration, all of which can adversely affect the strength development and durability of concrete. Thus, the overall water content in concrete, both from mixing water and that retained in the internal curing agent, becomes more important for low w/c concrete. In this context, it is crucial to first determine the accurate water absorption capacity of the internal curing materials. If the absorption capacity of a material is overpredicted, extra water would be released into cement paste at an early mixing stage. This would likely increase the w/c of the cement paste and might eventually result in unexpected consequences such as lower strength [10, 14].

Despite the importance of accurate water absorption capacity measurement, there are no standards or recommendations that are suitable for fine, highly absorptive materials such as activated carbon whose absorption capacity reaches around 100~200% of its mass. For example, ASTM C 128 describes a method to find the absorption of fine aggregate. However, this method is suitable to be applied for regular fine aggregate whose absorption capacity is generally less than 3% and is not suitable for highly absorptive material that has a high surface area and complex pore structure. Sometimes, tea-bag test is used for superabsorbent polymer [7, 15, 16]. This method, however, cannot effectively exclude water retained between and on particles or the water absorbed by the tea bag itself. Zhao et al. have proposed that interstitial water could affect absorption capacity of SAP [17]. Paper towel method (ASTM C 1761) can be used for lightweight aggregate, but it can only be applied to coarse aggregate and the measurement error appears to be relatively large [18].

Unlike the above methods that used water, Johansen et al. [10] suggested a method using isothermal calorimetry to examine the absorption capacity of an internal curing agent. The assessment occurs in cement-based materials, so pore solution rather than water is used. Also, compared to other methods that physically measure the amount of water absorbed, this method measures the heat of hydration of samples, which is a chemical indication of the rate of cement hydration. By comparing the early heat of hydration data of varying w/c pastes with that of a paste containing an internal curing agent, the amount of water absorbed by the internal curing agent can be determined. The detailed methodology can be found in Johansen et al. [10]. Later, Castro et al. [19] used a similar approach to assess water absorbed by fine lightweight aggregate but by comparing total heat release.

Although the isothermal calorimetry method seems to overcome the shortcomings of the previous methods, several improvements can be made in order to apply it to different

circumstances. First, the method assumes that the high surface area of the highly absorptive material does not alter the shape of rate of hydration curve. However, this may not hold true for some materials. That is, highly absorptive materials often have high pore volume and pore surface area. The surface area of the pores can act as nucleation sites for cement hydration that can potentially accelerate the cement hydration reaction. For instance, the addition of nanoparticles of TiO_2 , which have a high surface area, to cement paste accelerates cement hydration and alters the shape of rate of hydration curve [20]. Thus, materials that have high surface area due to pores could potentially affect the rate of cement hydration, which violates the main assumption of this method. When this happens, the shape of the rate of hydration curve is affected by both the surface area of the pores and the water content in the system, leading to misinterpretation of the results. Secondly, although it is an advantage to assess the absorption capacity within cement-based materials, these methods do not consider the effect of w/c of the paste when examining the absorption capacity. For example, the material would absorb more pore solution at higher w/c than at lower w/c , resulting in higher absorption capacity value.

This study aims to improve the method proposed by Johansen et al. [10] using multiple variables to accommodate different highly absorptive materials and different conditions. The detailed objectives of this study are to examine (1) the effect of different pore structures of the highly absorptive materials on the effective absorption capacity, and (2) the effect of w/c used on the effective absorption capacity.

In this paper, the terminology “effective absorption capacity” (EAC) is used [21]. It is based on the assumption that an absorptive material would absorb pore solution only up to a state where moisture equilibrium is reached within the matrix. For example, high-strength concrete mixed at low w/c would not have abundant pore solution available for internal curing agent to absorb, and some pores will remain empty. The EAC is defined as follows:

$$EAC = \frac{M_{EQ} - M_{OD}}{M_{OD}} \times 100\%. \quad (1)$$

Here, M_{OD} represents mass of a material at oven-dry condition and M_{EQ} represents mass of a material at moisture equilibrium state. The EAC value can change when the moisture state changes. In comparison, conventionally used terminology “absorption capacity (k)” is calculated using mass at saturated-surface-dry condition (SSD) rather than at moisture equilibrium state, representing a material’s true capacity for water absorption. The absorption capacity is a fixed value. For example, when an absorptive material is mixed into cementitious materials, the moisture state between the material and the cement paste gets equilibrated in the early stage of hydration. If the material is at SSD, the material cannot retain the maximum amount of water but releases some until moisture equilibrium is reached with cement paste. This not only lowers the absorptive potential of the internal curing agent, but also increases the water content in the cementitious matrix unexpectedly, which

might cause other serious problems. Thus, for the material that is expected to be used within another material, such as internal curing agents, the conventional definition of absorption capacity is not relevant. Rather, the amount of moisture that a material retains at moisture equilibrium state, as represented by EAC value, becomes more important. In most cases, the EAC value would be less than the conventional absorption capacity unless the base material has a relative humidity of 100%. The EAC value would likely be dependent on the w/c of the base material because cement paste with lower w/c would draw more water from the absorptive material. This is investigated as the second objective of this study.

2. Materials and Experimental Procedure

2.1. Materials. The highly absorptive materials used for this study are activated carbon fibre (ACF) and powdered activated carbon (PAC). These materials have a similar composition, which is mostly carbon, and are processed to have small, low-volume pores. The major difference between the two in terms of absorption capacity is their pore structure. Thus, any influence of using materials with different compositions can be minimized, while the pore structure is the only variable. The ACF used was ACF-1603-10 (Kynol Activated Carbon Fiber, Gunei Chemicals). This type of ACF has been widely used for research. The average fibre length is 3 mm and fibre diameter is $10\ \mu\text{m}$, as stated by the manufacturer. This type of ACF is produced by carbonization and gasification of a phenolic resin precursor. The PAC used is produced from coal, passing #325 mesh, as stated by the manufacturer. Particle size analysis was performed on PAC using ethanol as a dispersant (Mastersizer 2000, Malvern). The particle size distribution of PAC is shown in Figure 1.

Both materials were analysed by gas sorption analysis (3Flex, Micromeritics) to examine their pore characteristics. Pore size distribution was calculated by NLDFT method and is presented in Figure 2.

In Figure 2, the incremental pore volume is presented in terms of pore width. In the case of ACF, a single sharp peak was observed at pore width of 0.8-0.9 nm and most of the pore widths were below 1 nm. Considering that microporous materials contain pores with diameters less than 2 nm, ACF can be classified as microporous material. Compared to that, PAC showed a broader pore size distribution, beyond the limit of micropore range and extending to the mesopore range. The Brunauer-Emmett-Teller (BET) surface area was calculated to be $960\ \text{m}^2/\text{g}$ and $837\ \text{m}^2/\text{g}$ for ACF and PAC, respectively. Both of the materials were dried in an oven at 105°C for 24 hours to completely dry moisture in all the pores. Then they were stored separately in sealed containers until experiments were conducted.

The cement used in this study conforms to ASTM C 150 Type I Portland cement. The cement was analysed by X-ray fluorescence. The oxide composition of the cement analysed is presented in Table 1. Deionized water with $18.2\ \text{M}\Omega\ \text{cm}$ resistivity was used as mixing water. Polycarboxylate superplasticizer (SP) was used in some of the pastes for workable consistency of the pastes.

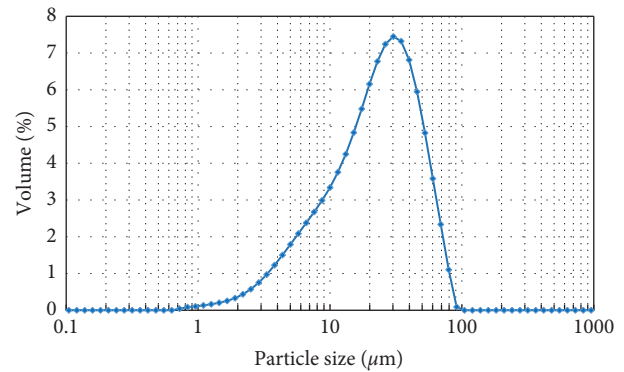


FIGURE 1: Particle size distribution of powdered activated carbon.

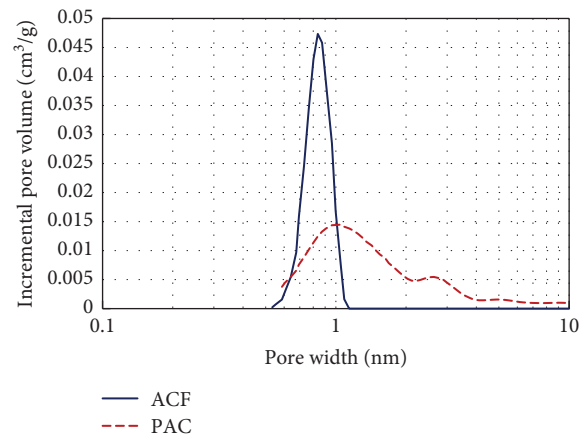


FIGURE 2: Pore size distribution of ACF and PAC.

TABLE 1: Chemical oxide analysis of cement.

Oxide/phase	Wt%
Silicon dioxide (SiO_2)	21.17
Aluminium oxide (Al_2O_3)	4.53
Iron oxide (Fe_2O_3)	3.68
Calcium oxide (CaO)	61.47
Magnesium oxide (MgO)	4.16
Titanium oxide (TiO_2)	0.3
Sodium oxide (Na_2O)	0.18
Potassium oxide (K_2O)	0.9
Manganic oxide (MnO)	0.12
Phosphorus pentoxide (P_2O_5)	0.21
Loss on ignition (LOI)	3.26
Total	99.98

2.2. Mix Design. As stated in Introduction, this paper comprises two parts. The first part examines the influence of different pore structures in determining the effective absorption capacity. The second part investigates the effect of the water-to-cement ratio of the paste on the effective water absorption capacity.

2.2.1. Part 1: Investigation into Pore Structure. In the first part of the study, the two materials with different pore structures, ACF and PAC, were used to study the influence

of their pore structure on EAC. Note that the pores of ACF are in the micropore range (pore diameter smaller than 2 nm), while those of PAC are in the micropore range and mesopore range (pore diameter larger than 2 nm and smaller than 50 nm). Cement pastes containing each of these materials, as well as neat cement paste (REF) as a reference sample, were prepared for isothermal calorimetry. The ACF and PAC were added at 1% of the mass of the cement. In this study, the amount of mixing water is divided into two classes. The amount of water used for cement hydration is referred to as “base water.” The amount of water that should be added to accommodate the amount that is absorbed by either ACF or PAC is referred to as “additional water.” For this part of the study, fixed w/c was used at 0.30, calculated using only base water. Iterations were performed by varying the amount of additional water because the EACs of these materials at this w/c are not known yet. In order to achieve workable consistency, polycarboxylate superplasticizer was used. This type of superplasticizer is known to retard the cement hydration process [22], which affects the shape of the rate of hydration curve. Thus, the same dosage of superplasticizer was used for every comparative sample set, including the reference sample. For example, the same amount of superplasticizer was used for both ACF containing cement paste and the reference sample. This enabled a qualitative comparison within the same set of experiment. The mixing proportions of the first part are shown in Table 2.

2.2.2. Part 2: Investigation into w/c . For the second part examining the effect of different w/c on the EAC, only activated carbon fibre was utilized. Three w/c s were used: 0.25, 0.30, and 0.40. The ACF was added at 1% of the mass of the cement. In this part, PAC was not used because the current methodology was found to be not suitable for a mesoporous material as will be demonstrated later. The mixing proportions of the samples were calculated in the same manner as in the first part of the study and are presented in Table 3.

2.3. Mixing. The mixing procedure was as follows. To prepare the samples, all materials and mixing equipment were equilibrated at $25 \pm 2^\circ\text{C}$ for 24 hours before testing. Cement paste samples containing ACF or PAC were prepared along with the control ordinary Portland cement paste sample. For the samples that included ACF or PAC, the particles were submerged in a premeasured amount of total water (base water and additional water) for 5 minutes to give the materials some time to absorb water. In this step, superplasticizer was added. Cement was then added and mixed using a hand-held mixer.

2.4. Heat Release Measurement and EAC Calculation. In both parts of this study, isothermal calorimetry was used (I-Cal 2000 HPC, Calmetrix) to measure the heat of cement hydration at 25°C . The authors have performed multiple experiments with this equipment and obtained sufficiently reproducible results, verifying that it is suitable for this

study. After mixing, 100 ± 5 g of the samples were put in a plastic container and placed in the calorimeter less than 10 minutes after the mixing of water with cement. The calorimetry data of the initial 1 hour were excluded to allow the samples to become equilibrated within the instrument. Measurements were made up to the initial 24 hours from the start of mixing. The rate of hydration curves of these pastes will be compared to determine the EAC of the ACF and PAC mostly following the method proposed by Johansen et al. [10]. When the rate of the hydration curve for ACF or PAC paste coincides with that of REF at a certain value of additional water, it is inferred that the material has absorbed all of the additional water and the moisture equilibrium is reached within the matrix at $w/c = 0.30$. Now, EAC can be calculated by dividing additional water by oven-dry mass of a material.

3. Results and Discussion

3.1. Effect of Pore Structure on the Effective Absorption Capacity. The first part of this study examined the effect of pore structure in determining the EAC of a porous material, when used within a cementitious matrix. In this part, the rate of hydration curves of ACF- and PAC-containing cement pastes are compared at $w/c = 0.30$. The isothermal calorimetry results for the ACF and PAC are presented in Figures 3(a) and 3(b), respectively.

It is found in Figure 3(a) that the rate of hydration curve of a sample that was mixed with 150% additional water (ACF-150%-30) almost overlapped with that of REF. This indicates that all the “additional water” stays within the pores of ACF during early hydration and that the cement only uses “base water” for hydration. This results in similar curve to that of the REF of the same w/c . It can be considered that the moisture equilibrium is reached between the ACF and the cement paste at $w/c = 0.30$. In case of ACF-200%-30, higher amount of additional water resulted in the shift of the curve to the right. The excess water is expected to increase the w/c of the overall matrix, and moisture equilibrium would be reached at higher w/c . In general, higher w/c slows the early hydration reaction, shifting the peak to the right [10, 19]. On the other hand, the case of lower amount of additional water (ACF-120%-30) resulted in the shift of the curve slightly to the left. Thus, the effective absorption capacity of the ACF is found to be 150% at this w/c and addition rate used.

Here, it should be noted that the curves of ACF-150%-30 and REF overlap very well despite ACF having a huge BET surface area. It was observed in another study that huge surface area of nano- TiO_2 that had been added to cementitious materials altered the rate of hydration curve by acting as nucleation sites for cement hydration products [23]. For example, the addition of 5% TiO_2 to cement paste accelerated cement hydration and increased the peak rate of hydration. Compared to that, the higher BET surface area of ACF does not seem to affect the shape of the hydration curve. The authors presume that this is related to small pore radius of ACF. There is a study suggesting that the hydration products cannot precipitate in pores with diameters smaller

TABLE 2: Mixing proportions for part 1 (relative mass).

Absorptive material	Notation	Cement	ACF	PAC	Total water		SP
					Base water	Additional water	
ACF	REF	100	0	0	30	0.0	0.8
	ACF-120%-30	100	1	0	30	1.2 (120%)	0.8
	ACF-150%-30	100	1	0	30	1.5 (150%)	0.8
	ACF-200%-30	100	1	0	30	2.0 (200%)	0.8
PAC	REF	100	0	0	30	0.0	1.0
	PAC-160%-30	100	0	1	30	1.6 (160%)	1.0
	PAC-200%-30	100	0	1	30	2.0 (200%)	1.0
	PAC-240%-30	100	0	1	30	2.4 (240%)	1.0

TABLE 3: Mixing proportions for part 2 (relative mass).

Notation	Cement	ACF	Total water		SP
			Base water	Additional water	
REF	100	0	25	0.0	1
100%-25	100	1	25	1.0 (100%)	1
130%-25	100	1	25	1.3 (130%)	1
200%-25	100	1	25	2.0 (200%)	1
REF	100	0	30	0.0	0.8
120%-30	100	1	30	1.2 (120%)	0.8
150%-30	100	1	30	1.5 (150%)	0.8
200%-30	100	1	30	2.0 (200%)	0.8
REF	100	0	40	0.0	0
0%-40	100	1	40	0.0 (0%)	0
100%-40	100	1	40	1.0 (100%)	0
200%-40	100	1	40	2.0 (200%)	0

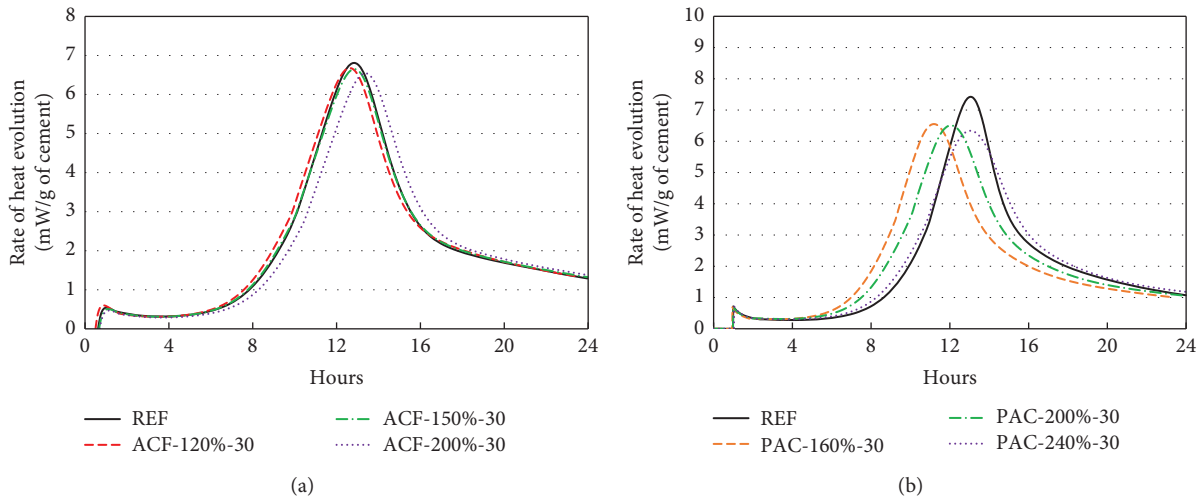


FIGURE 3: Rate of hydration curves of cement pastes: (a) REF- and ACF-containing cement pastes with 120%, 150%, and 200% additional water; (b) REF- and PAC-containing cement pastes with 160%, 200%, and 240% additional water.

than about 2 nm [24]. Also, Kupwade-Patil et al. suggest that the size of a globule and its aggregates is expected to be in the range of ~ 1 nm to $10 \mu\text{m}$ at an early age of the cement hydration reaction, studied by Ultra-Small Angle X-Ray Scattering (USAXS) [25]. This indicates that hydration products would not likely precipitate in pores that are

smaller than 1 nm. Considering that the pore size of ACF is mostly less than 1 nm, the hydration products would have not formed inside the micropores of ACF. In other words, the micropores act as water reservoirs but do not act as surface area for hydration product nucleation sites. As the micropores are the major cause of the huge BET surface area

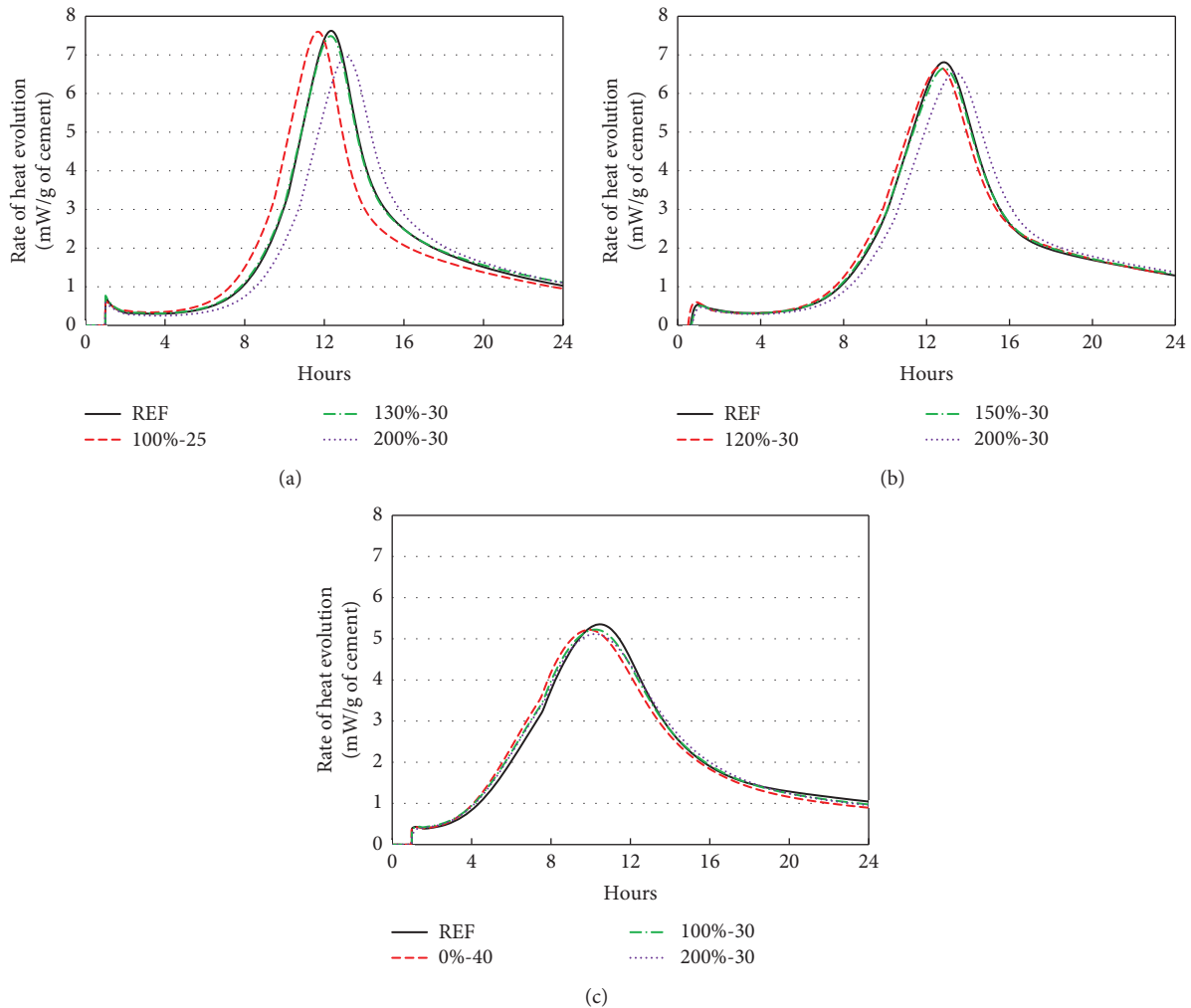


FIGURE 4: Rate of hydration curves of ACF-containing cement pastes: (a) $w/c = 0.25$ with 100%, 130%, and 200% additional water, (b) $w/c = 0.30$ with 120%, 150%, and 200% additional water, and (c) $w/c = 0.40$ with 0%, 100%, and 200% additional water.

of ACF, the BET value does not seem to have contributed to the change in the rate of the hydration process. Also, considering the micron scale size of the ACF, the authors presume that the outer surface area be too small to alter the shape of the rate of hydration curve.

On the other hand, in Figure 3(b), none of the rate of hydration curves of PAC-containing pastes overlap with that of REF for the amounts of additional water examined in this study. The curves shifted to the right with higher amounts of additional water as expected, implying that moisture equilibrium between PAC and cement paste were reached at higher w/c . However, the peak heights were lower than that of REF. The mismatch in the shape of the rate of hydration curves indicates that there have been changes in the cement hydration mechanism due to the addition of PAC. Considering that PAC does not take part in chemical hydration process, it is hypothesized that the surface area of PAC took part in the hydration reaction mechanism. As shown in Figure 2, the pore diameters of PAC are in the range of micropore and mesopore. This suggests that cement hydration products can crystallize and grow within the larger

pores, meaning that the surface area of the pores could act as nucleation sites for cement products to hydrate, affecting the rate of cement hydration reaction. This is a distinctive difference between ACF and PAC. The mesopores of PAC seem to affect the rate of hydration curve not only by participating in moisture equilibrium but also by presumably providing extra surface area. Due to the added variable other than the w/c , the effective absorption capacity of PAC cannot be reasonably predicted using the isothermal calorimetry method.

3.2. Effect of w/c on the Effective Absorption Capacity. In the second part, three water-to-cement ratios were compared at 0.25, 0.30, and 0.40 in order to examine whether the water content in cement paste affects the effective absorption capacity of an absorptive material. The isothermal calorimetry results for $w/c = 0.25, 0.30,$ and 0.40 are presented in Figures 4(a)–4(c), respectively. Figure 4(b) is reproduced from Figure 3(a) to better compare the trend between the three w/cs examined.

In Figure 4(a), it is found that the rate of hydration curve of the ACF-cement paste with 130% additional water (130%-25) almost coincides with that of REF. Two curves match not only at the peak, but also in the acceleration and deceleration zones. This indicates that the cement paste, excluding ACF and water absorbed by the ACF, hydrates the same as REF. Thus, the effective absorption capacity of ACF can be concluded as 130% at this w/c used. The additional water at 200% of the mass of ACF (200%-25) resulted in the shift of the curve to the right compared to the REF curve. On the other hand, the additional water at 100% of the mass of ACF (100%-25) resulted in the shift of the curve to the left compared to the REF curve. This trend is similar to Figure 3(a), where higher additional water was linked to moisture equilibrium at higher w/c . That is, higher w/c and thus excess amounts of water tend to retard the hydration process and lower the peak rate of heat release, and vice versa, as stated in 3.1.

Recalling that the EAC value was determined as 150% at $w/c = 0.30$ (Figure 3(a)), the one obtained here at $w/c = 0.25$ shows a lower value of 130%. This implies that the effective absorption capacity of a material can be different at different w/c used. This can be explained by the equilibrium of moisture state between cement paste and the absorptive material. At higher w/c , water is more abundant throughout the cement paste. The absorptive material should retain more water to maintain moisture equilibrium with the cement paste. Thus, the effective absorption capacity tends to increase. This suggests that the EAC value can change according to w/c used. When using the isothermal calorimetry method to find the effective absorption capacity of an absorptive material, the most accurate result can be acquired when the w/c used for isothermal calorimetry is the same as the w/c that will be used for the end purpose.

Comparing Figures 4(a)–4(c), the curves are more congested around REF curve as the w/c increases. For example, curves of 100%-25 and 200%-25 are clearly separated from that of REF (Figure 4(a)) but curves of 100%-40 and 200%-40 almost overlap with that of REF (Figure 4(c)). In fact, the rates of hydration curves for the $w/c = 0.4$ case do not show meaningful differences, and it was not possible to find the EAC. It is obvious that the lower w/c allows for better examination of the EAC. This is related to the amount of water that is needed to fully complete hydration reaction of cement, known approximately at $w/c = 0.30$ – 0.35 . At low w/c , cement is in need of water for hydration. So small change in water content is directly related to hydration reaction. At high w/c , on the other hand, cement already has water for hydration; thus small change in water content does not effectively alter the hydration curve. It is recommended that the w/c be less than 0.40 to be able to examine the EAC using the isothermal calorimetry method.

4. Conclusions

In this study, isothermal calorimetry method was used to determine the effective absorption capacity of absorptive materials. Several factors were investigated that could affect the EAC value. It was found that the effective absorption

capacity of a material that has micropores (ACF) can be determined by the isothermal calorimetry method. However, the effective absorption capacity of a material that has both micropores and mesopores (PAC) was not successfully predicted. It is presumed that surface area of mesopores affects the shape of the rate of cement hydration. This could interfere with the effect of moisture equilibrium, leading to improper interpretation of the effective absorption capacity. Also, it was found that lower w/c is related to lower EAC when this method is used. At lower w/c , absorptive material would absorb less water and reach moisture equilibrium at lower w/c . It is recommended that the w/c less than 0.40 be used, so that rates of hydration curves are clearly distinguished and more accurate EAC can be obtained.

Data Availability

The data used to support the findings of this study are available from the corresponding author upon request.

Conflicts of Interest

The authors declare that there are no conflicts of interest regarding the publication of this paper.

Acknowledgments

This study was supported by a research grant from the University of Suwon in 2017.

References

- [1] R. Philleo, "Concrete science and reality," *Materials Science of Concrete*, pp. 1–8, American Ceramic Society, Westerville, OH, USA, 1991.
- [2] D. P. Bentz and K. A. Snyder, "Protected paste volume in concrete: extension to internal curing using saturated lightweight fine aggregate," *Cement and Concrete Research*, vol. 29, no. 11, pp. 1863–1867, 1999.
- [3] D. Cusson and T. Hoogeveen, "Internal curing of high-performance concrete with pre-soaked fine lightweight aggregate for prevention of autogenous shrinkage cracking," *Cement and Concrete Research*, vol. 38, no. 6, pp. 757–765, 2008.
- [4] A. Bentur, S.-I. Igarashi, and K. Kovler, "Prevention of autogenous shrinkage in high-strength concrete by internal curing using wet lightweight aggregates," *Cement and Concrete Research*, vol. 31, no. 11, pp. 1587–1591, 2001.
- [5] S. T. Yildirim, C. Meyer, and S. Herfellner, "Effects of internal curing on the strength, drying shrinkage and freeze–thaw resistance of concrete containing recycled concrete aggregates," *Construction and Building Materials*, vol. 91, pp. 288–296, 2015.
- [6] S.-I. Igarashi and A. Watanabe, "Experimental study on prevention of autogenous deformation by internal curing using super-absorbent polymer particles," in *Proceedings of the International RILEM Conference on Volume Changes of Hardening Concrete: Testing and Mitigation*, Lyngby, Denmark, August 2006.
- [7] S.-H. Kang, J. Moon, and S.-G. Hong, "Effect of internal curing by super-absorbent polymer (SAP) on hydration, autogenous shrinkage, durability and mechanical

- characteristics of ultra-high performance concrete (UHPC),” *Journal of the Korea Concrete Institute*, vol. 28, no. 3, pp. 317–328, 2016.
- [8] J. Justs, M. Wyrzykowski, D. Bajare, and P. Lura, “Internal curing by superabsorbent polymers in ultra-high performance concrete,” *Cement and Concrete Research*, vol. 76, pp. 82–90, 2015.
- [9] P. Jongvisuttisun, C. Negrello, and K. E. Kurtis, “Effect of processing variables on efficiency of eucalyptus pulps for internal curing,” *Cement and Concrete Composites*, vol. 37, pp. 126–135, 2013.
- [10] N. A. Johansen, M. J. Millard, A. Mezencevova, V. Y. Garas, and K. E. Kurtis, “New method for determination of absorption capacity of internal curing agents,” *Cement and Concrete Research*, vol. 39, no. 1, pp. 65–68, 2009.
- [11] M. Suzuki, M. S. Meddah, and R. Sato, “Use of porous ceramic waste aggregates for internal curing of high-performance concrete,” *Cement and Concrete Research*, vol. 39, no. 5, pp. 373–381, 2009.
- [12] P. Jongvisuttisun and K. E. Kurtis, “The role of hardwood pulp fibers in mitigation of early-age cracking,” *Cement and Concrete Composites*, vol. 57, pp. 84–93, 2015.
- [13] O. M. Jensen and P. Lura, “Techniques and materials for internal water curing of concrete,” *Materials and Structures*, vol. 39, no. 9, pp. 817–825, 2006.
- [14] T. Hammer, “High strength LWA concrete with silica fume effect of water content in the LWA on mechanical properties,” *Supplementary Papers in the Fourth CANMET/ACI International Conference on Fly Ash, Silica Fume, Slag, and Natural Pozzolans in Concrete: Istanbul, Turkey, 1992*, CANMET/ACI, Indianapolis, IN, USA, 1992.
- [15] S.-H. Kang, S.-G. Hong, and J. Moon, “Absorption kinetics of superabsorbent polymers (SAP) in various cement-based solutions,” *Cement and Concrete Research*, vol. 97, pp. 73–83, 2017.
- [16] C. Schröfl, V. Mechtcherine, and M. Gorges, “Relation between the molecular structure and the efficiency of superabsorbent polymers (SAP) as concrete admixture to mitigate autogenous shrinkage,” *Cement and Concrete Research*, vol. 42, no. 6, pp. 865–873, 2012.
- [17] S. Zhao, O. M. Jensen, and M. T. Hasholt, “Measuring absorption of superabsorbent polymers in cementitious environments,” *Materials and Structures*, vol. 53, no. 1, p. 11, 2020.
- [18] E. Albert, I. V. Miller, R. Spragg et al., “Determining the moisture content of pre-wetted lightweight aggregate: assessing the variability of the paper towel and centrifuge methods,” in *Proceedings of the 4th International Conference on the Durability of Concrete Structures*, West Lafayette, IN, USA, July 2014.
- [19] J. Castro, I. D. L. Varga, and J. Weiss, “Using isothermal calorimetry to assess the water absorbed by fine LWA during mixing,” *Journal of Materials in Civil Engineering*, vol. 24, no. 8, pp. 996–1005, 2012.
- [20] B. Y. Lee, A. R. Jayapalan, and K. E. Kurtis, “Effects of nano-TiO₂ on properties of cement-based materials,” *Magazine of Concrete Research*, vol. 65, no. 21, pp. 1293–1302, 2013.
- [21] B. Y. Lee, “Effective absorption capacity of highly absorptive materials using isothermal calorimetry, considering the effect of specific surface area,” *Journal of the Architectural Institute of Korea Structure & Construction*, vol. 34, no. 2, pp. 49–56, 2018.
- [22] F. Puertas, H. Santos, M. Palacios, and S. Martínez-Ramírez, “Polycarboxylate superplasticiser admixtures: effect on hydration, microstructure and rheological behaviour in cement pastes,” *Advances in Cement Research*, vol. 17, no. 2, pp. 77–89, 2005.
- [23] B. Y. Lee and K. E. Kurtis, “Influence of TiO₂ nanoparticles on early C₃S hydration,” *Journal of the American Ceramic Society*, vol. 93, no. 10, pp. 3399–3405, 2010.
- [24] K. K. Aligizaki, *Pore Structure of Cement-Based Materials: Testing, Interpretation and Requirements*, Crc Press, Boca Raton, FL, USA, 2005.
- [25] K. Kupwade-Patil, S. Chin, J. Ilavsky, R. N. Andrews, A. Bumajdad, and O. Büyüköztürk, “Hydration kinetics and morphology of cement pastes with pozzolanic volcanic ash studied via synchrotron-based techniques,” *Journal of Materials Science*, vol. 53, no. 3, pp. 1743–1757, 2018.

Research Article

Influence of the Amount of Steel Fibers on Fracture Energy and Drying Shrinkage of HPRCC

Weina Guo ¹, Peng Zhang ¹, Yupeng Tian,¹ Bing Wang,² and Wan Ma¹

¹Center for Durability & Sustainability Studies of Shandong Province, Qingdao University of Technology, Qingdao 266033, China

²Qingdao Municipal Construction Group, Qingdao 266000, China

Correspondence should be addressed to Peng Zhang; peng.zhang@qut.edu.cn

Received 26 February 2020; Revised 30 May 2020; Accepted 1 June 2020; Published 20 June 2020

Guest Editor: Rishi Gupta

Copyright © 2020 Weina Guo et al. This is an open access article distributed under the Creative Commons Attribution License, which permits unrestricted use, distribution, and reproduction in any medium, provided the original work is properly cited.

The fracture energy of the high-performance fiber-reinforced cement-based composite (HPRCC) can be modified within wide limits by the variation of the amount of steel fibers added to the fresh mix. First of all, considering the actual engineering conditions in Qingdao, the materials commonly used in Qingdao were selected. The optimal reference mix proportion of the HPRCC cementing material was proposed through determination of fluidity and flexural strength. Based on the optimal mix proportion, the uniaxial tensile, fracture, and dry shrinkage properties of HPRCC with different steel fibers are systematically studied. Stress-strain diagrams of the different samples were measured under the uniaxial tensile test, wedge splitting test, and three-point bending test. The steel fiber content was varied between 0 and 200 kg/m³. The load bearing capacity and the fracture energy were determined experimentally. In addition, moisture loss as a function of time and shrinkage was determined in an environment of 20°C and 50% RH (relative humidity). The results indicate that the maximum load increases significantly in the HPRCC series reinforced by 150 and 200 kg/m³ of steel fibers. Both have a hardening branch developed after the first crack deflection due to the high percentage of fibers bridging the crack surfaces. The load bearing capacity and fracture energy increased almost linearly with the steel fiber content. It was found that the three-point bending test is more applicable in measuring the fracture energy of HPRCC than the wedge splitting test. The addition of steel fibers decreased the moisture diffusion and consequently the drying shrinkage of HPRCC, and there was minimum weight loss and deformation when the steel fiber content was 150 kg/m³. The results obtained will be presented and discussed.

1. Introduction

Concrete is the most widely used building material, but its brittleness increases with its strength. Adding fiber into concrete can effectively improve the brittleness of concrete and improve its own crack resistance. At present, the fibers often added in the cement matrix are mainly steel fibers, glass fibers, synthetic fibers, natural fibers, and so on, and among them, the steel fiber is the most widely used [1–11]. The related research results show that the addition of the steel fiber into the cement matrix can greatly improve the fracture toughness and fracture energy of concrete [12–16]. To further improve the compactness and mechanical properties of concrete, in addition to adding steel fibers, fine pozzolanic reaction additives such as fly ash and silica fumes are also added [17–28]. Due to the pozzolanic reaction and filling, the

composite further achieves a more compact structure, which is called HPRCC [29–32]. Because of its compact structure, it has high strength, high durability, low porosity, and good volume stability [29, 33–37]. HPRCC is a new type of cementitious material which appeared in the mid-1990s [38]. It has the characteristics of low water-binder ratio, superhigh molding, and so on [39, 40]. Compared to the ordinary concrete, HPRCC has a very high compressive strength of 100–800 MPa, tensile strength of 20–50 MPa, elastic modulus of 50–60 GPa, and fracture energy up to 40 kJ/m² [41–44]. At present, HPRCC is the most prospective construction material for both civil and military structures, such as for nuclear waste storage, containment, fortification, highway bridge, and municipal and high-rise buildings [39, 45–49].

At home and abroad, the mechanical properties, durability, volume stability, microstructure, and preparation

technology of HPRCC have been studied extensively [50–55]. There are also many research studies on the fracture energy of HPRCC. Sovják et al. [56] studied the relationship between the effective fracture energy and the strain rate of HPRCC with different steel fiber volume contents and concluded that the higher the fiber volume content, the lower the strain rate sensitivity. Nguyen et al. [57] studied the effect of different types of steel fibers on the fracture energy of steel fiber-reinforced concrete, and the results showed that the ratio of elastic fracture energy to total fracture energy was the lowest, ranging from 0.02 to 0.08, and the local fracture energy and total fracture energy was the highest, ranging from 0.38 to 0.82. Ren et al. [39] studied the influence of different steel fiber contents and types on the fracture energy and fracture toughness of ultrahigh-performance cement-based composites. The results showed that the steel fiber contents and types had a great influence on the fracture toughness and fracture energy. Tran et al. [6] analyzed the fracture energy of UHPRC at a strain rate of $5\text{--}92\text{ s}^{-1}$ and obtained a specimen with a fiber content of 1–1.5% with a very high fracture energy ($28\text{--}71\text{ kJ/m}^2$). In the above literature, the influence of different types of steel fibers on the fracture performance of HPRCC was mainly studied. While the targeted research on the change of steel fiber content in HPRCC from its fracture energy and dry shrinkage is relatively less, they are essential to improve the service performance of the structure and the collapse resistance of the structure under extreme load or environments, especially.

To fully understand the influence of different steel fiber content on the fracture and dry shrinkage properties of HPRCC, this paper first uses Qingdao local materials as the base material and obtains the best mix proportion of the matrix materials through the fluidity and flexural strength test; then, the steel fiber is added on the basis of this best mix proportion and is made into the HPRCC studied in this paper. Firstly, the fracture energy of HPRCC with different contents of steel fiber is studied and analyzed by using the wedge splitting method and the three-point bending method recommended by the RILEM [58] and China DL/T5332-2005 “Norm for fracture test of hydraulic concrete” [59]. In addition, the dry shrinkage performance of HPRCC was studied and analyzed at 20°C and 50% RH. Then, the load crack opening displacement curve, fracture energy, and dry shrinkage performance of HPRCC with different steel fibers are compared and analyzed, and the influence of HPRCC with different steel fiber content on the fracture performance and dry shrinkage performance is discussed, which lays a solid foundation for HPRCC to be widely used in practical projects.

2. Experimental Details and Methods

2.1. Materials and Mix Proportions. For the tests described in this contribution, HPRCC with five different amounts of steel fibers (SF) varying between 0 and 200 kg/m^3 has been prepared. Ordinary Portland cement (OPC) Type 42.5, fly ash (FA) class F with an average particle diameter of $5.4\text{ }\mu\text{m}$, and silica fumes with an average particle size of

$0.03\text{ }\mu\text{m}$ were used to produce the test samples. The chemical compositions of OPC, silica fumes, and fly ash are summarized in Table 1. In addition, fine quartz sand (Q_s) with a grain size of 0.2 to 0.35 mm and quartz powder (Q_p) with a maximum grain size of $45\text{ }\mu\text{m}$ were added. The composition of the matrix was optimized in a systematic way. Copper-plated steel fibers (SFs) with a length of 13 mm and a diameter of 0.2 mm were added to the fresh mix, the properties of the steel fiber in this paper are listed in Table 2, and the shape of the steel fibers is shown in Figure 1. Ordinary tap water is used as the mixing water. To improve the workability of the mix, the superplasticiser (SP) was added. The superplasticiser (SP) is a polycarboxylate superplasticiser from Jiaozhou (Qingdao, China), and its water reduction rate and solid content are 25% and 20%, respectively. The compositions of the specimens are given in Table 3. In addition, ordinary cement mortar test blocks were made for the comparative study of the fracture energy of HPRCC. The materials of ordinary cement mortar test blocks were ordinary Portland cement (PO 32.5), river sand after sieving (maximum size is 5 mm), and tap water. The naming forms of specimens with different mix proportions are shown in Table 4. The proportion and its mechanical properties are shown in Table 5.

2.2. Preparation of Test Specimens. All the raw materials poured into the mixer in sequence (quartz powder, fly ash, silica fume, cement, and quartz sand) are stirred evenly. And then, 80% water and superplasticisers were mixed evenly which were slowly added to the mixture at a low mixing speed, followed by pouring 20% water directly into the mixture. The steel fibers were then slowly added to the mixture at a low mixing speed within one minute, followed by a medium mixing speed for three minutes to achieve uniform fiber dispersion. The fresh mixture was cast into the corresponding moulds and vibrated on the vibration table for three minutes. The whole mixing process of materials is shown in Figure 2. After compaction in the steel form on a vibrating table, the specimens were allowed to harden in the laboratory covered with plastic sheets for 24 hours. Then, they were further cured in hot water at 80°C for 72 hours. And then, all specimens were removed and cured in a humid chamber at $T = 20 \pm 2^\circ\text{C}$ and $\text{RH} > 95\%$ before testing.

2.3. Fluidity and Flexural Strength Test. The fluidity of the fresh mixture is determined by the reciprocating flow table method, and the specific experimental method is in accordance with the GB/T2419-2016 “Test method for fluidity of cement mortar.” When the specimens are obtained from curing at the corresponding age, their flexural strength is measured with a cement mortar testing machine, with reference to the standard GB/T17671-2019 “Method of testing cement determination of strength.” The optimal mix ratio of HPRCC was determined from the results of fluidity and flexural strength and was applied to the subsequent experimental study.

TABLE 1: Chemical composition of ordinary Portland cement (OPC), silica fumes, and fly ash (FA) (%).

Type	CaO	SiO ₂	Al ₂ O ₃	Fe ₂ O ₃	SO ₃	K ₂ O	Na ₂ O	TiO ₂
OPC	60.09	20.90	6.55	5.43	2.44	1.61	1.07	0.01
Silica fumes	0.98	95.64	0.40	0.22	0.18	1.51	0.20	0.02
FA	1.78	49.75	36.81	5.93	0.31	1.78	0.25	2.29

TABLE 2: Properties of steel fiber (SF).

Type	L/D	L (mm)	D (mm)	f_t (MPa)	E (GPa)	ρ (g/m ³)
SF	65	13	0.2	2600	200	8.0

Note. SF: steel fiber; L/D: length to diameter ratio; L: length; D: diameter; f_t : tensile strength; E: elastic modulus; ρ : density.



FIGURE 1: The shape of steel fibers.

2.4. Uniaxial Tensile Test. A dumbbell-shaped specimen was used for the uniaxial tensile test [60, 61]. The size of the was specimen determined by the Japanese norms (Recommendations for the Design and Construction of High-Performance Fiber-Reinforced Cement Composites with Multiple Fine Cracks), as shown in Figure 3. The test was carried out on a Shimadzu AG-TS 250 kN universal testing machine with a maximum load of 250 kN. The beam displacement accuracy was 0.001 mm, the loading accuracy was 0.01 kN, and the beam moving speed was 0.1 mm/min. Two linear variable displacement transducers (LVDTs) affixed to a testing frame were used to measure the deformation of specimens. The specimen deformation value can be obtained from the average of the reading from the left and right sides of LVDTs. LVDT installation location is shown in Figure 3.

2.5. Uniaxial Compression Test. Specimens of 100 mm × 100 mm × 300 mm were cast for the determination of static strength. The shape of the specimen for the compression test is shown in Figure 4. Three samples of each batch were tested. The compressive strength measurements were conducted according to GB/T 17671-2005 (similar to ISO 697:1989) [62]. The test was carried out by a Changchun Vinte electro-hydraulic servo universal testing machine,

with a maximum load of 2000 kN, a beam displacement accuracy of 0.001 mm, and a load accuracy of 0.001 kN. The test machine is set to control the loading in a load mode with a loading rate of 0.1 MPa/s. The centering and preloading process were repeated until the test specimen is completely centered and meets the preloading requirements, and then the uniaxial compression test is performed. The uniaxial compression test is performed in the displacement mode with a loading rate of 0.001 mm/s. The load is measured by a load sensor with a range of 2000 kN, the deformation is measured by the strain gauge, and the average value of the readings on the left and right sides is taken as the deformation value of the specimen.

2.6. Wedge Splitting Test. Specimens 200 mm (length) × 200 mm (height) × 40 mm (width) were used for the wedge splitting test as shown in Figure 5 [58]. The initial crack is reserved for casting, and the initial seam height ratio is $a/H = 0.5$. The test device for wedge splitting is the same as the uniaxial tensile test device. An extensometer with a precision of 0.001 mm is placed on each side of the specimen to measure the crack opening displacement. The crack opening displacement value can be obtained from the average of the reading from the left and right sides of the extensometer. And then, the steel split joint is placed in the notch of the test piece, and the beam is moved and adjusted so that the wedge-shaped steel plate connected to the beam just contacts the split joint pulley. At that moment, the test is started, the load is controlled by displacement control loading, and the loading rate is 0.3 mm/min. The load and crack deformation readings are automatically recorded by the computer.

2.7. Three-Point Bending Test. The standard prism specimen of 160 mm (length) × 40 mm (height) × 40 mm (width) was used for the three-point (3-P) bending test [63, 64]. The initial crack is reserved for casting, and the initial seam height ratio is $a/H = 0.5$. The specimens were placed on the frame of three-point bending. The rigid frame and force on the specimen are shown in Figure 6. The test device for the three-point bending test is the same as the uniaxial tensile test device and the wedge splitting test device, and controlled loading is done with a displacement rate of 0.3 mm/min. In the test process, the load and the displacement of the loading point are recorded by the computer connected to the testing device.

2.8. Drying Shrinkage. In addition, some standard prisms with dimensions of 160 mm (length) × 40 mm (height) × 40 mm (width) have been cured in a water bath at 80°C for 72 hours after demoulding. They were then put in a standard curing room with $T = 20 \pm 2^\circ\text{C}$ and $\text{RH} > 95\%$ until the age of 28 days. After that, the specimens were placed in the laboratory with the atmosphere of 20°C and 50% RH for three months. The time-dependent moisture loss and drying shrinkage have been measured for these HPRCC specimens.

TABLE 3: The best mix selection range for HPFRCC.

W/B	Cement	Silica fumes	Fly ash	S/B	Quartz powder	SP
0.19–0.21	0.5–1	0.25–0.35	0–0.5	0.68–1.08	0.27–0.47	0.01

TABLE 4: Mix proportions of specimens.

Name	W/B	OPC	Silica fumes	FA	Quartz sand	Quartz powder
A ₁	0.19	1	0.25	0	0.88	0.37
A ₂	0.2	1	0.25	0	0.88	0.37
A ₃	0.21	1	0.25	0	0.88	0.37
A ₄	0.22	1	0.25	0	0.88	0.47
B ₁	0.21	1	0.15	0	0.88	0.42
B ₂	0.21	1	0.2	0	0.88	0.37
B ₃	0.21	1	0.25	0	0.88	0.32
B ₄	0.21	1	0.3	0	0.88	0.27
B ₅	0.21	1	0.35	0	0.88	0.37
C ₁	0.21	1	0.25	0	0.68	0.37
C ₂	0.21	1	0.25	0	0.78	0.37
C ₃	0.21	1	0.25	0	0.88	0.37
C ₄	0.21	1	0.25	0	0.98	0.37
C ₅	0.21	1	0.25	0	1.08	0.37
D ₁	0.21	1	0.25	0	0.88	0.37
D ₂	0.21	0.9	0.25	0.1	0.88	0.37
D ₃	0.21	0.8	0.25	0.2	0.88	0.37
D ₄	0.21	0.7	0.25	0.3	0.88	0.37
D ₅	0.21	0.6	0.25	0.4	0.88	0.37
D ₆	0.21	0.5	0.25	0.5	0.88	0.37

TABLE 5: Mix proportion and mechanical properties of ordinary cement mortar specimens.

Water-binder ratio	Cement (kg/m ³)	Sand (kg/m ³)	Water (kg/m ³)	Flexural strength (MPa)	Compressive strength (MPa)
0.5	450	1350	225	5.86	34.6

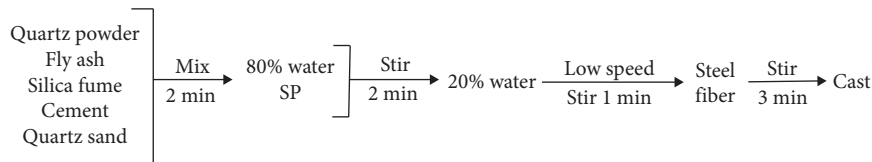


FIGURE 2: HPFRCC mixing process.

3. Results and Discussion

3.1. Fluidity and Flexural Strength. Through fluidity and flexural strength tests, the effects of HPFRCC fluidity and flexural strength at different water-to-binder ratios ($W/B = 0.19, 0.2, 0.21, \text{ and } 0.22$), silica fume contents ($0.15, 0.20, 0.25, 0.30, \text{ and } 0.35$), sand-binder ratios ($0.68, 0.78, 0.88, 0.98, \text{ and } 1.08$), and replacement quantity of fly ash ($0, 0.1, 0.2, 0.3, 0.4, \text{ and } 0.5$) were obtained. The specific results are shown in Figure 7.

In addition to the sand-binder ratio, when the water-binder ratio, silica fume content, and fly ash replacement amount increase, the fluidity of the mixture increases linearly as can be seen in Figure 7. When the water-to-binder ratio is 0.21, the mixture can quickly fill the mould under the action of vibration, and a large number of bubbles appear on

the surface of the mixture during the vibration. After the fracture of the test piece, there are no holes in the cross section of the test piece, and the flexural strength is only 5.9% lower than that of the water-binder ratio 0.2. The reason is that the increase in the mixing water increases the pores between the particles. When the amount of silica fumes is large, the fluidity of the mixture increases. This is mainly because the silica fume particles are spherical, the particles are very small, and the quartz powder particles are irregular in shape and are polygonal. Therefore, when the silica gel ratio is increased, the fluidity is also increased. The fluidity and flexural strength of the mixture are the largest, when the content of the silica fumes is 0.35 and quartz powder is 0.27. When the sand-binder ratio increases, the fluidity of the mixture decreases clearly, while the flexural strength of the specimen increases first and then decreases; when the sand-

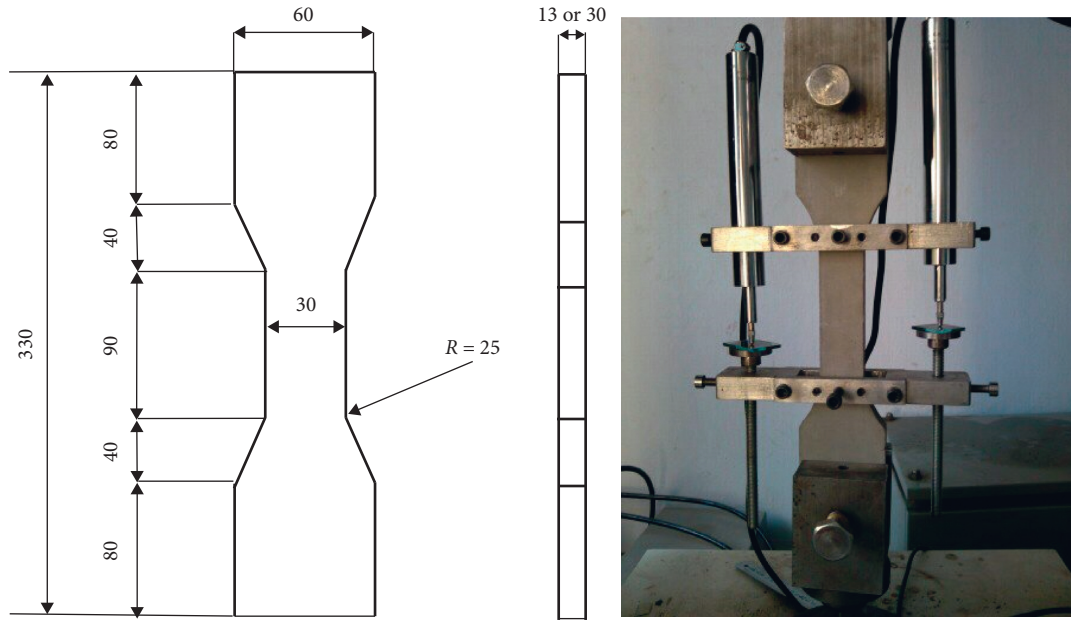


FIGURE 3: Uniaxial tensile test (mm).

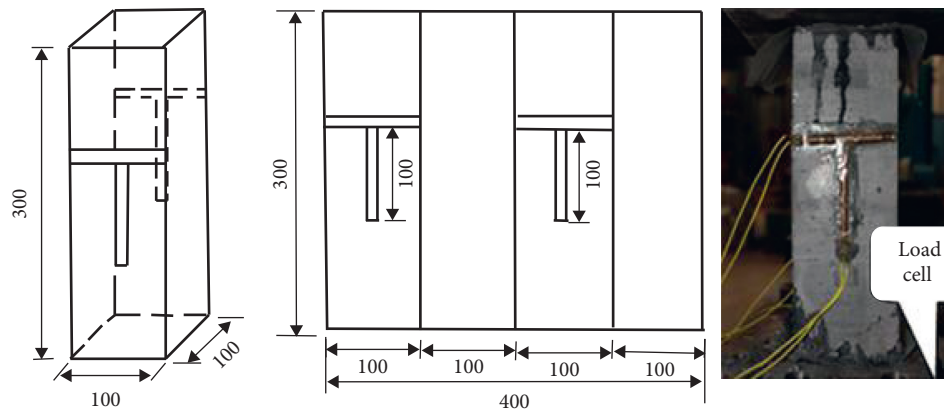


FIGURE 4: Uniaxial compression test specimen (mm).

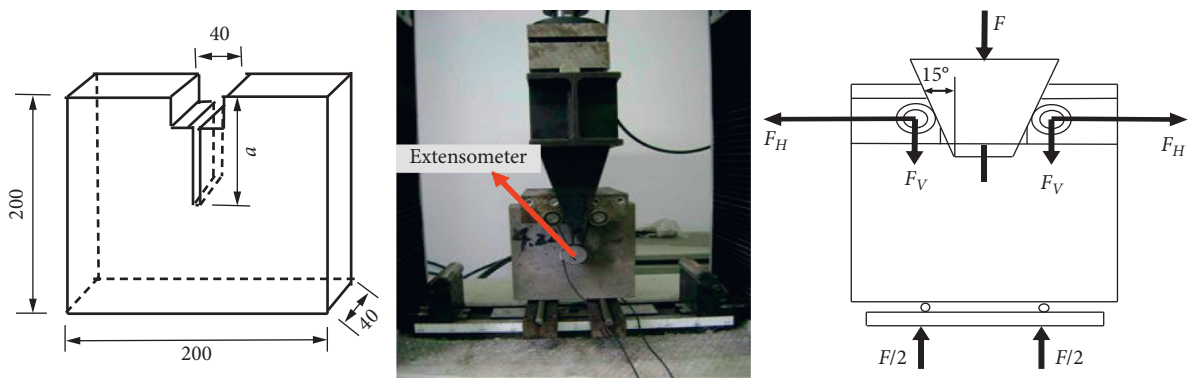


FIGURE 5: Wedge splitting test (mm).

binder ratio is 0.68 and 0.88, the strength is 9.2% and 13.3%, which is lower than that of 0.78, mainly because there are particles of different sizes in the granular material system

and the smaller particles have filling effect. The amount of cement replaced by fly ash increases, and its flexural strength increases first and then decreases; when it is 30%, the

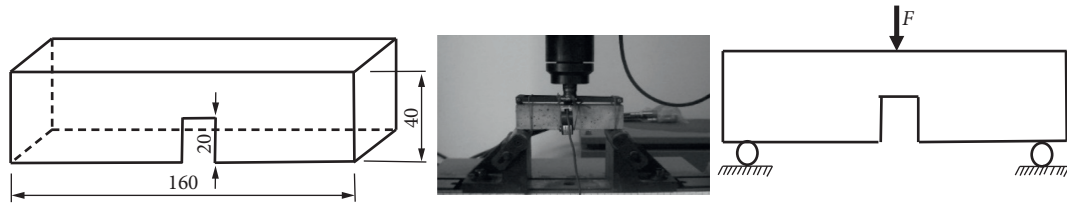


FIGURE 6: Three-point bending test (mm).

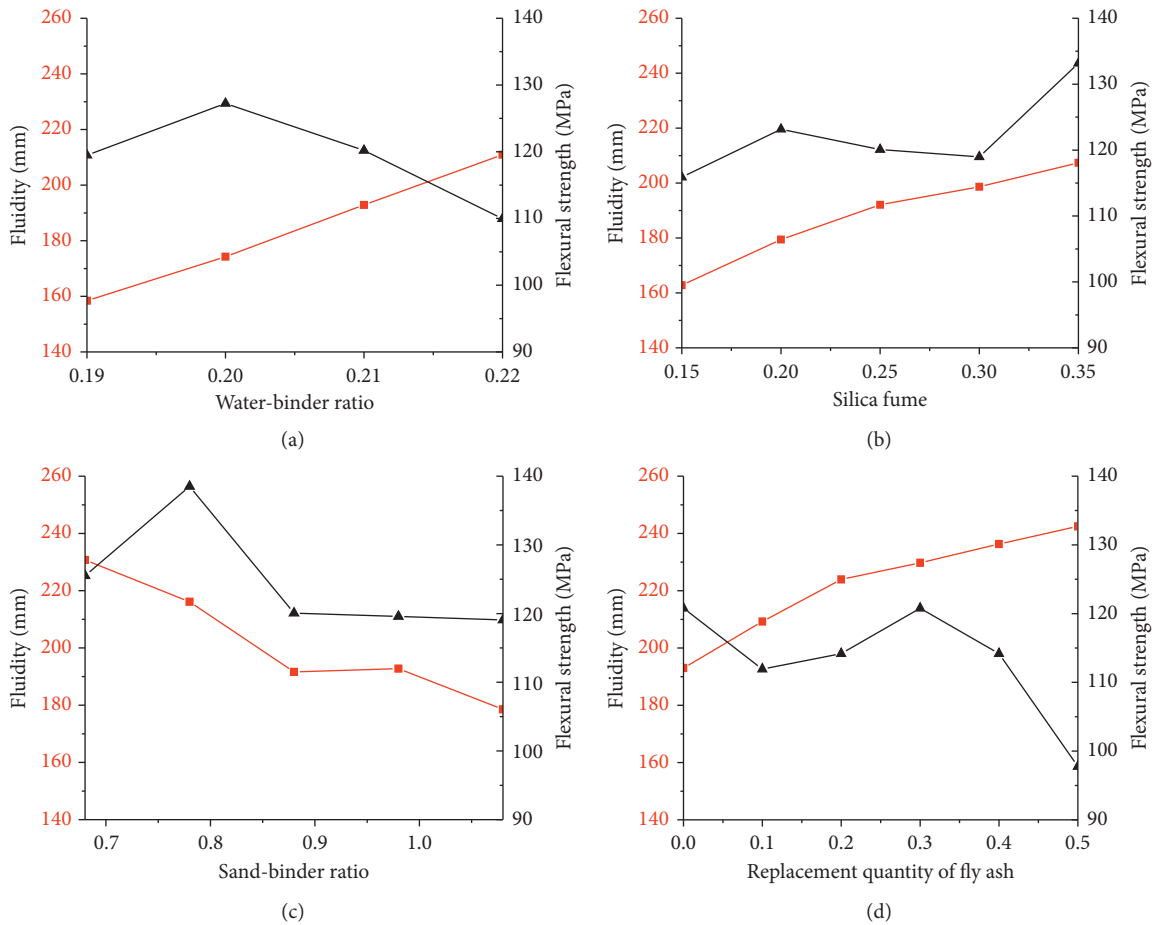


FIGURE 7: Effect of different variables on fluidity and flexural strength of HPCRCC.

strength of the specimen reaches the highest. Compared with the substitution number of 0, the strength of HPCRCC increases by 1.2%, but the fluidity of the mixture increases by 41 mm, up to 233 mm, and this is mainly because the reaction of fly ash to produce calcium hydroxide is earlier than that of cement hydration, and the strength of the calcium aluminate hydrate produced by the two reactions is lower than that of calcium silicate hydrate.

To sum up, considering the fluidity and flexural strength comprehensively, the optimal combination of HPCRCC obtained from the test is as follows: water-binder ratio is 0.21 and cement:silica fume:fly ash:quartz sand:quartz powder = 0.7:0.35:0.3:0.78:0.27.

3.2. Tensile Stress-Strain Behavior. Figure 8 illustrates the tensile stress-strain behavior of HPCRCC with different steel fiber behavior. Obviously, after the HPCRCC specimen is mixed with steel fibers, the initial stage of tension is still the elastic stage, and the stress increases linearly with the increase in strain. The ultimate tensile strength of HPCRCC increases continuously with the increase in the steel fiber content. The main reason is that the steel fiber has the ability to hinder and restrain the crack growth, so the ultimate tensile strength is improved.

It can be seen from the tensile test results of HPCRCC that when the steel fiber is added to HPCRCC, its tensile initial stage is still elastic, and the stress increases linearly

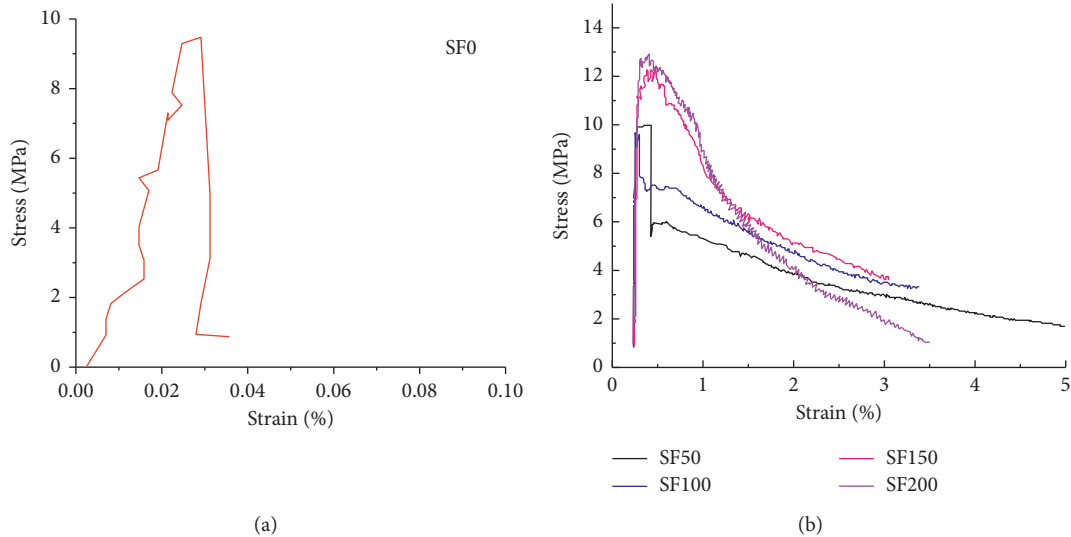


FIGURE 8: Tensile stress-strain diagrams of HPFRCC with different amount of steel fibers.

with the increase in strain. With the increase in the steel fiber content, the ultimate tensile strength of HPFRCC increases. The main reason is that the steel fiber can effectively prevent crack growth. As can be seen from Figure 8, when the steel fiber is not added, the stress of the specimen reaches the ultimate tensile strength and starts to drop vertically until the specimen fails. At this time, cracks appear in the sample, which is divided into two parts, showing obvious brittle characteristics. And, with the increase in steel fibers, the stress reduction section becomes slower and longer, which is mainly due to the continuous consumption of energy during the extraction process of steel fibers, which significantly improves the fracture resistance of the test piece. It can be concluded that the incorporation of steel fibers into HPFRCC can significantly improve the tensile strength of the material, increase the deformation capability of the material, and improve the ductility of the material, making it from brittle failure to plastic failure.

3.3. Compressive Strength. The uniaxial compression test was performed on HPFRCC specimens with a steel fiber content of 0–200 kg/m³, and the compressive strength of the samples is shown in Figure 9.

It can be seen from Figure 9 that the steel fiber has a greater impact on the compressive strength of HPFRCC. With the increase in the steel fiber content, the compressive strength increases approximately linearly, and the increase rate is approximately unchanged when the steel fiber content is 0–150 kg/m³, but when the amount of steel fiber is increased from 150 kg/m³ to 200 kg/m³, the increase rate slows down. This is mainly due to the good mechanical occlusion between steel fibers and the base material, which can improve the compressive strength of HPFRCC to a certain extent. However, with the increase in the amount of the steel fiber, the distribution of the steel fiber is uniform, and the inside of the specimen does not become dense, which causes the growth rate of compressive strength of HPFRCC to slow

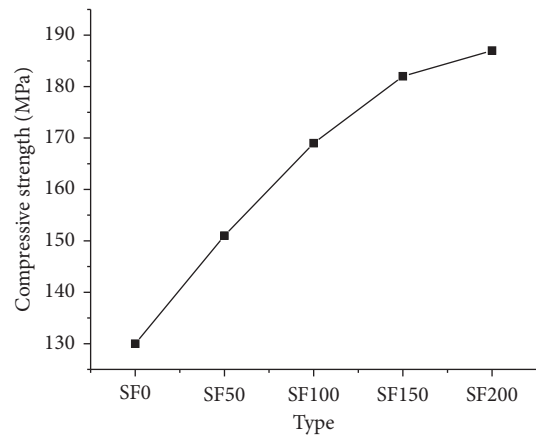


FIGURE 9: The compressive strength of HPFRCC with different steel fiber content.

down. Therefore, in the range of 0–200 kg/m³, as the steel fiber content increases, the compressive strength does not increase linearly.

3.4. Results of Wedge Splitting Test. Firstly, the load-CMOD curves of cement mortar and HPFRCC specimens obtained by the wedge splitting test are compared. In Figure 10, different colors represent the test data obtained from three different samples with the same content of the steel fiber. From Figure 10, compared with HPFRCC without steel fiber, the peak load of the cement mortar test block is similar, but the crack opening displacement of HPFRCC is significantly larger than that of the ordinary cement mortar, so the fracture energy of HPFRCC is significantly higher than that of the ordinary cement mortar. However, during the test, it can be seen that when the load of the common cement mortar reaches the peak value, small cracks appear along the direction of the main cracks, and then the cracks gradually extend to a certain length with the wedge-shaped plate, and

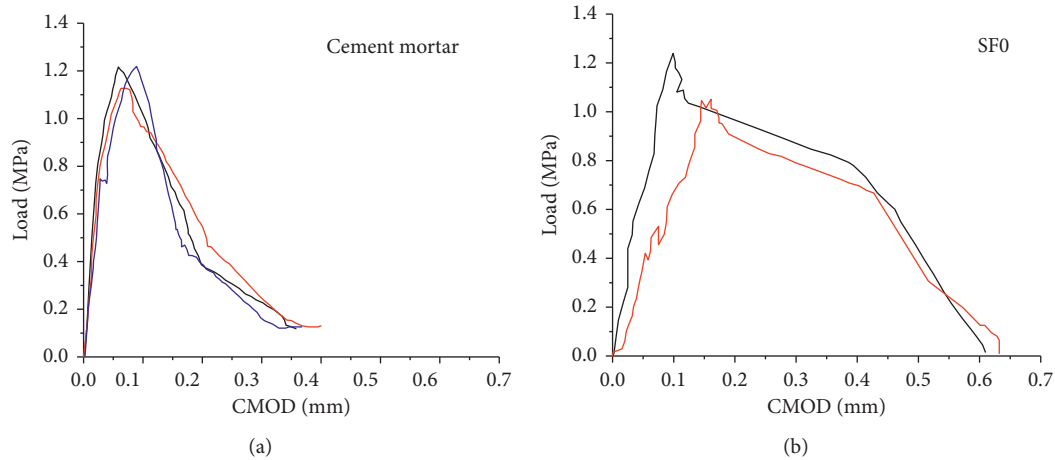


FIGURE 10: Load-CMOD curves of cement mortar and HPFRCC without steel fibers.

the specimen suddenly cracks into two halves. When the HPFRCC test specimen without the addition of steel fibers reaches the peak load, the test specimen suddenly shows brittle fracture along the main crack without any indication, indicating that HPFRCC is more brittle than the ordinary cement mortar, which is mainly due to its pure fine aggregates.

The fracture properties of HPFRCC with different content of steel fibers are further studied. The test results obtained by the wedge split test are shown in Figure 11 (the steel fiber content of 50 kg/m^3 could not be recorded due to the testing machine and operator). As can be seen from Figure 11(a), the stress of all specimens can be divided into three stages: crack initiation stage, crack propagation stage, and instability failure stage. From the load-CMOD curves, it can be seen that after the curve passes through the peak point, it descends approximately linearly in a gentle slope, which is very different from the curve of the ordinary mortar specimen. This is mainly due to the uniform and disordered distribution of the steel fiber inside the specimen after mixing with the steel fiber, so that the specimen does not fully develop along the direction of the main crack reserved in the specimen after reaching the cracking load, but at the same time, there are transverse cracks, which can also be obtained from the corresponding failure image of the specimen (Figure 11(b)). From the corresponding failure pictures, it is evident that with the increase in the steel fiber content, the crack opening displacement increases gradually. The main reason is that the steel fiber consumes the energy of crack growth in the process of slowly pulling out, which makes its fracture resistance significantly improved.

From Figure 11(b), it can be seen that there are many transverse cracks in the sample due to the existence of the steel fiber. It is mainly due to the uneven distribution of the steel fiber in the sample. To a certain extent, it shows that the wedge-shaped split test is not suitable for the experimental study of fracture performance of HPFRCC materials.

In the wedging split test, the maximum splitting force of the cement mortar specimen and the HPFRCC specimen was obtained, as shown in Figure 12.

It should not be ignored that compared with the cement mortar test block, the maximum splitting force of HPFRCC with the steel fiber is significantly increased. With the increase in the steel fiber content, the maximum splitting force increases significantly, mainly due to the good tensile strength of the steel fiber and good mechanical bite force with the matrix. During the failure of the test piece, the steel fiber exerted its tensile performance better, thereby increasing the maximum splitting force of the HPFRCC specimen.

3.5. Results of Three-Point Bending Test. By using the three-point bending test to study the fracture performance of HPFRCC specimens with different steel fiber content, the test results are obtained as shown in Figure 13. The data in the figure are the average of the test results of three different samples with the same steel fiber content.

As can be seen from the figure, compared with the HPFRCC without steel fiber, the bearing capacity of HPFRCC with steel fiber is significantly enhanced, which is mainly due to the addition of the steel fiber, which increases the toughness and crack resistance of the specimen. Compared with the load-deformation curve of the specimen with a steel fiber content of $50\text{--}200 \text{ kg/m}^3$, it is obtained that as the amount of steel fiber increases, the fuller the load-deformation curve, the peak load and deformation also gradually increase, and the area under the curve gradually increases, i.e., the fracture energy increases. The main reason is that with the increase in the steel fiber content, the number of fibers per unit area increases, which increases the bonding force between the fiber and the matrix and improves the positive ability of the specimen. At the same time, the energy of crack growth is consumed in the process of slow drawing, which improves the fracture resistance of the steel fiber significantly.

The calculation formulas of fracture energy, characteristic length, and ductility index is shown in formulas (1)–(3) [65–67]. Also, the performance indicators for each mix ratio in the three-point bending test are shown in Table 6.

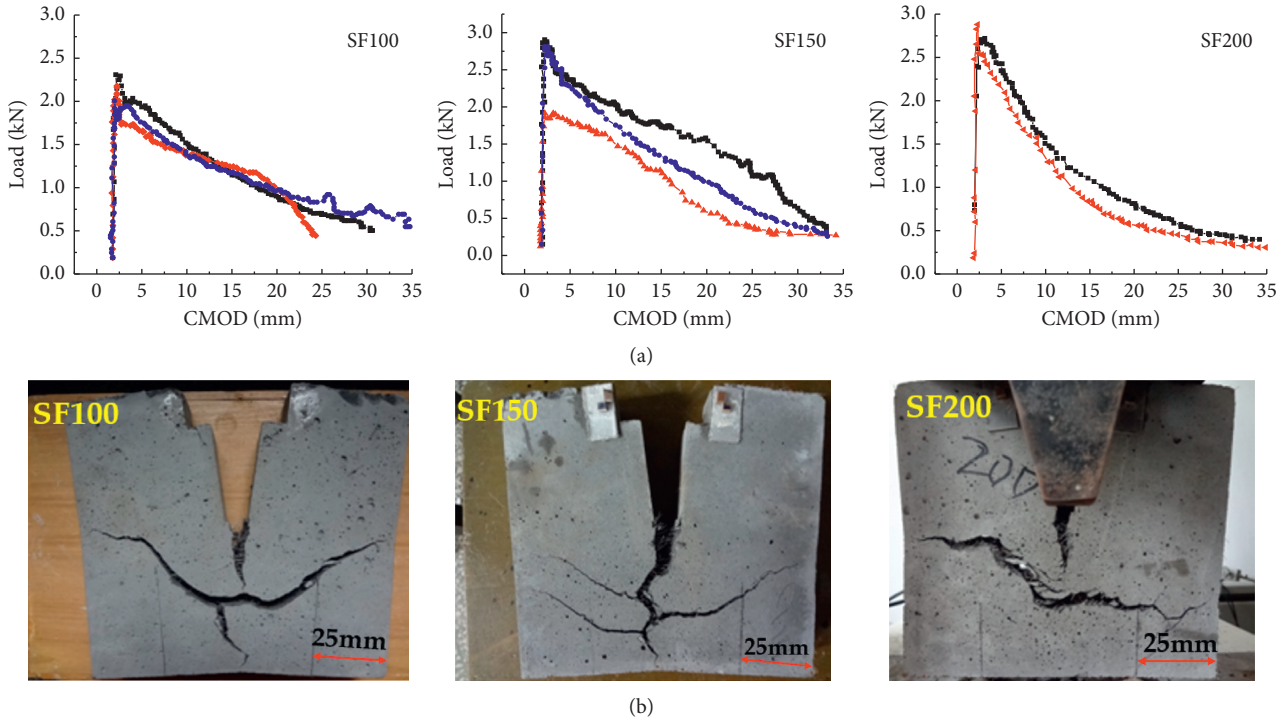


FIGURE 11: (a) The load-CMOD curves of HPRC with 100 kg/m³ to 200 kg/m³ of steel fibers during the wedge splitting test. (b) Cracking form of a specimen with different contents of steel fibers.

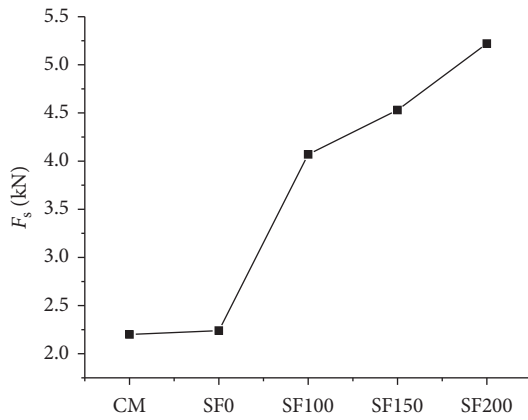


FIGURE 12: The maximum splitting force for different specimens.

$$G_f = \frac{W_0 + W\delta_0}{A_{lig}}, \quad (1)$$

$$l_{ch} = \frac{G_f E}{(f_t)^2}, \quad (2)$$

$$D_u = \frac{G_f}{P_{max}}, \quad (3)$$

where W_0 is the area under the load-CMOD (or deflection) curves up to rupture of the specimen (N·mm), W stands for the deadweight of the specimen, δ_0 is the maximum

deflection, A_{lig} is the surface area of the broken ligament (mm²), E is the elastic modulus, f_t is the tensile strength of the materials, and P_{max} is the maximum load.

It can be seen from Figure 14 that the maximum load, fracture energy, characteristic length, and ductility index of HPRC notched beams increase significantly after the addition of steel fibers. Compared to that without the steel fiber, the maximum load, fracture energy, characteristic length, and ductility index are increased about 1–5 times, 100–320 times, 100–190 times, and 60–70 times, respectively. It can be seen that the effect of strengthening and toughening with steel fibers are very obvious. It can also be seen from the test results that the two indexes of characteristic length and ductility index do not have a unified trend with the increase in the steel fiber content, and they reach the highest when the steel fiber content is 100 kg/m³ and 50 kg/m³, respectively. However, the ductility index has a little change after adding different quantities of steel fibers, which shows that the difference of the resistance to deformation of HPRC with a steel fiber content of 50 kg/m³ and 200 kg/m³ is not significant, and when HPRC is used for special purposes, the cost of materials can be greatly reduced.

It can be seen from Figure 14 that there is a clear linear relationship between deflection, maximum load, and fracture energy and steel fiber content. To verify this statement, a linear regression was performed on the relationship between each fracture index and the amount of steel fiber as shown in Table 7, and it was found that they follow the rules shown in Table 7.

From the formulas in the table, it can be seen that the maximum load, fracture energy, and deflection are linear

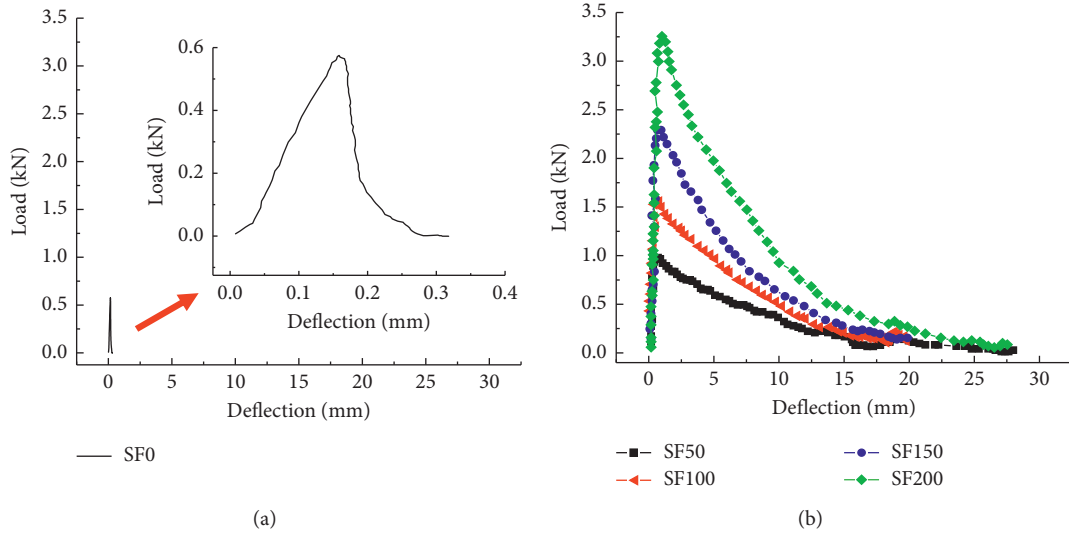


FIGURE 13: The load-deflection curves of HPRC with different amount of steel fibers between 0 and 200 kg/m³ obtained by the three-point bending test.

TABLE 6: Fracture performance indicators of HPRC.

Type	δ_0 (mm)	E (GPa)	P_{max} (kN)	G_f (J/m ²)	l_{ch} (m)	D_u (m ⁻¹)
SF0	0.3	42.41	0.642	92.11	0.049	0.143
SF50	17.85	43.16	1.031	10480	4.969	10.164
SF100	19.68	49.56	1.652	16034	8.257	9.705
SF150	21.83	40.64	2.303	19972	5.156	8.672
SF200	25.19	37.76	3.191	31744	7.550	9.942

Note. δ_0 : deflection; E : elastic modulus; P_{max} : maximum load; G_f : fracture energy; l_{ch} : characteristic length; D_u : ductility index.

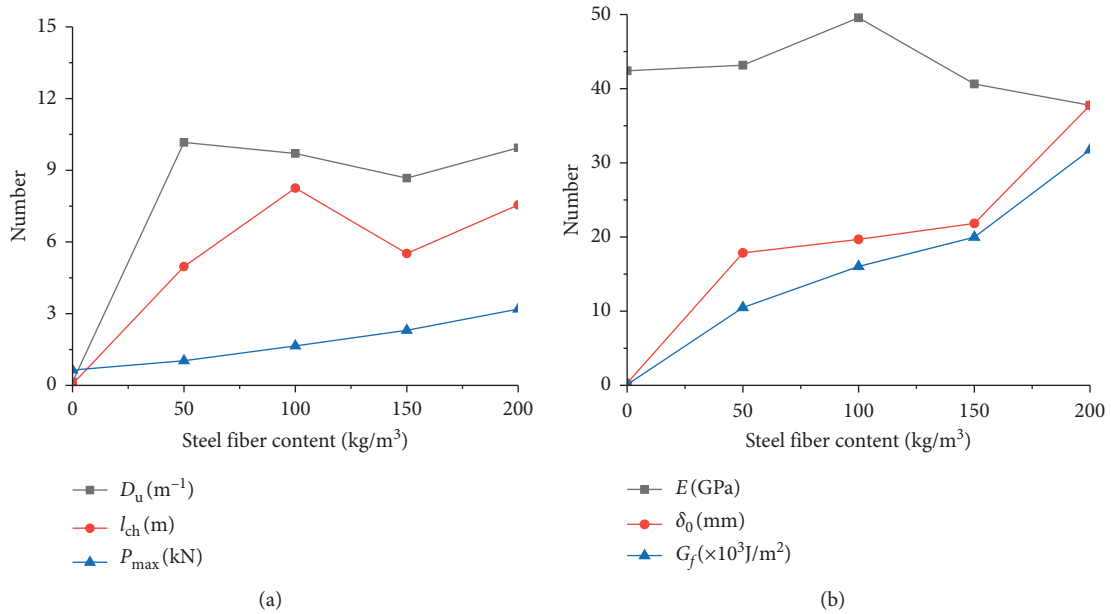


FIGURE 14: Relationship between fracture performance indicators and steel fiber content.

TABLE 7: Linear regression between fracture performance index and steel fiber content for HPCRCC.

Index	Regression equation	R^2	
$x = \text{steel fiber}$	$y = P_{\max}$	$y = 0.01274x + 0.4898$	0.97489
	$y = G_f$	$y = 145.59156x + 1105.266$	0.95927
	$y = \delta_0$	$y = 0.1075x + 6.218$	0.76622
	$y = E$	$y = -0.02364x + 45.07$	0.18383
	$y = l_{ch}$	$y = 0.04538x + 2.1732$	0.55651
	$y = D_u$	$y = 0.03621x + 4.104$	0.44805

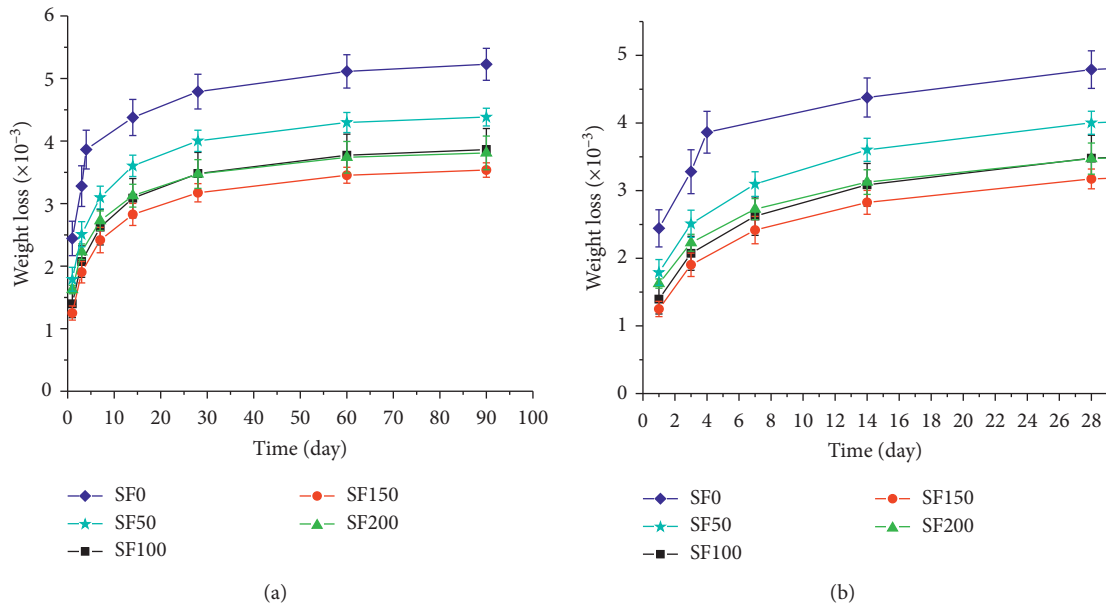


FIGURE 15: Weight loss of HPCRCC with different content of steel fibers under 50% RH and 20°C.

and positively related to the amount of the steel fiber. This indicates that the maximum load, fracture energy, and deflection increase with the increase in the steel fiber content, which proves that the addition of the steel fiber in HPCRCC can improve its own fracture energy carrying capacity and deformation capacity. The main reason is that a large amount of crack growth energy can be consumed during the process of steel fibers pull out, and its fiber bridging ability can effectively inhibit the development of cracks and fully exert its own tensile properties.

3.6. *Dry Shrinkage.* Figures 15 and 16 show the weight loss and shrinkage of the HPCRCC with different steel fiber contents under the conditions of 50% RH and 20°C through the dry shrinkage test.

It can be seen from Figure 15 that the weight loss rate of each mix proportioning specimen increases rapidly in the first 14 days under a dry environment, and the first 14 days is the most important period of weight loss. After 14 days, the weight loss of the specimen rises slowly with a small increase. Taking the test piece without the steel fiber as an example, when the drying age is 1 d, 3 d, 7 d, and 14 d, the weight loss rate of the test piece is 47%, 63%, 74%, and 84% of the 90 d water loss rate, respectively. This is mainly because the water

in the cement matrix diffuses from inside to outside, and the water lost in the early stage is mainly the water near the surface of the specimen. This part of water is easy to lose, and the loss rate is fast, while the water lost in the later stage is the water inside or even in the center of the test piece, which is difficult to spread, and the loss rate is slow.

It can also be seen from Figure 15 that, after adding steel fibers, the water loss rate of the test specimens at each dry age is smaller than that without steel fibers. The 90 d weight loss rates of steel fiber specimens mixed with 50 kg/m³, 100 kg/m³, 150 kg/m³, and 200 kg/m³ were 84%, 74%, 68%, and 73% of the water loss rate of the specimens without steel fibers. This is mainly due to the addition of steel fibers to HPCRCC, which is equivalent to replacing the same volume of matrix material with steel fibers in the test sample.

It can be seen from Figure 16 that the shrinkage deformation of specimens with different mix proportions increases rapidly in the first 14 days under a dry environment, and the first 14 days is the most important period of shrinkage deformation. After 14 days, the shrinkage deformation of the specimen rises slowly with a small increase. This is mainly because the dry shrinkage of the cement matrix is mainly caused by the loss of water. The more the loss of water, the greater the dry shrinkage deformation. The shrinkage deformation of specimens without steel fiber was

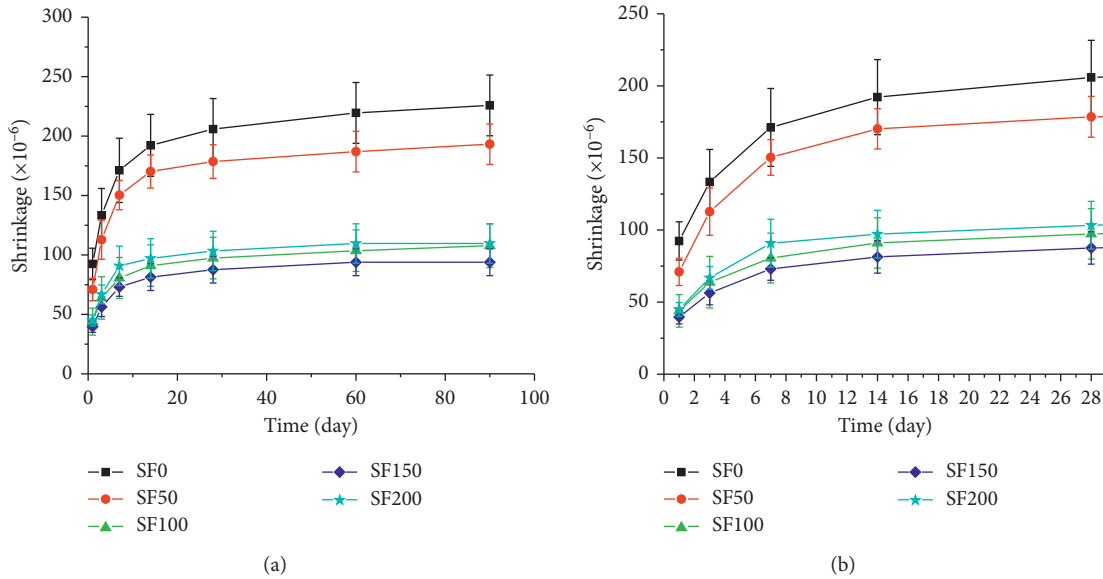


FIGURE 16: Shrinkage of HPCRCC with different content of steel fibers under 50% RH and 20°C.

41%, 59%, 76%, and 85% of the shrinkage deformation of 90 days, respectively, when the drying age was 1 d, 3 d, 7 d, and 14 d. The shrinkage deformation ratio was close to the water loss ratio. It can also be seen from Figure 16 that the shrinkage deformation value of the HPCRCC specimen with steel fibers is much smaller than that without steel fibers. At the same time, the slope of the shrinkage deformation curve of HPCRCC specimens with steel fibers is significantly lower than that of steel specimens without steel fibers after 28 days. This shows that the restriction of shrinkage and deformation after the incorporation of steel fibers is very effective.

4. Conclusions

In this paper, high-performance concrete with high strength and good working performance is made from Qingdao local materials. Based on this, a series of studies on the uniaxial tensile, fracture, and dry shrinkage properties of HPCRCC are carried out, and the following conclusions can be drawn:

- (1) The cement-based high-strength matrix is brittle, but fracture energy can be increased substantially by the addition of steel fibers. The composite material becomes more ductile, and the load bearing capacity increases.
- (2) It can be seen from the relationship between the content of steel fibers and the fracture performance indicators that with the increase in the steel fiber content, most fracture performance indexes (fracture energy G_f , deformation δ_0 , maximum load P_{max} , ductility index D_w , and characteristic length l_{ch}) increase. The fracture energy increases the most, which shows that the ductility and bearing capacity of HPCRCC can be significantly improved by increasing the steel fiber content.
- (3) The wedging split test shows that the brittleness of HPCRCC without steel fibers is much greater than

that of the ordinary cement mortar. After the steel fiber is added to the specimen, the stress in the specimen is distributed uniformly and disorderly, so that the crack does not fully develop along the direction of the main crack reserved in the specimen after the specimen reaches the cracking load, but at the same time, the transverse crack appears, and the ideal performance parameters are not obtained. This indicates that the wedging split test is not suitable for the study of the fracture performance of HPCRCC.

- (4) After adding steel fibers, the strengthening and toughening effect of HPCRCC are very obvious. The maximum load, fracture energy, characteristic length, and ductility index of notched beams are all increased significantly. Between them, the fracture energy and maximum load increased almost linearly with the steel fiber content.
- (5) The water loss and shrinkage deformation of HPCRCC increased rapidly in the first 14 days in the dry environment, and the first 14 days is the most important period of shrinkage. After 14 days, the weight loss and shrinkage deformation of HPCRCC increased slowly with little increase. But, the addition of steel fibers decreased the moisture diffusion, and consequently the drying shrinkage of HPCRCC.

Data Availability

The data used to support the findings of this study are available from the corresponding author upon request.

Conflicts of Interest

The authors declare that there are no conflicts of interest regarding the publication of this paper.

Authors' Contributions

Weina Guo was responsible for conceptualization, methodology, and writing—original draft preparation; Peng Zhang was responsible for examination, writing—review—and editing, supervision, and project administration.

Acknowledgments

This research was funded by the National Natural Science Foundation of China, grant numbers 51922052, 51778309, and U1706222; Natural Science Foundation of Shandong Province, grant number ZR2018JL018; Open Research Fund Program of State Key Laboratory of Hydrosience and Engineering, grant number SKLHSE-2019-C-04.

References

- [1] S. P. Shah and C. Ouyang, "Mechanical behavior of fiber-reinforced cement-based composites," *Journal of the American Ceramic Society*, vol. 74, no. 11, pp. 2727–2953, 1991.
- [2] A. Nanni and J. Aziz, "RCC pavement reinforced with steel fibers," *Concrete International*, vol. 11, no. 3, pp. 64–69, 1989.
- [3] V. S. Gopalratnam, S. P. Shah, B. Gordon et al., "Fracture toughness of fiber reinforced concrete," *ACI Materials Journal*, vol. 88, no. 4, pp. 339–353, 1991.
- [4] D. Soulioti, N. M. Barkoula, A. Paipetis, T. E. Matikas, T. Shiotani, and D. G. Aggelis, "Acoustic emission behavior of steel fibre reinforced concrete under bending," *Construction and Building Materials*, vol. 23, no. 12, pp. 3532–3536, 2009.
- [5] J. Matikas, A. Sharma, and K. Grauf, "Mechanical properties of concrete with steel and polypropylene fibres at elevated temperatures," *Fibers*, vol. 7, no. 2, 2019.
- [6] N. T. Tran, T. K. Tran, J. K. Jeon, J. K. Park, and D. J. Kim, "Fracture energy of ultra-high-performance fiber-reinforced concrete at high strain rates," *Cement and Concrete Research*, vol. 79, pp. 169–184, 2016.
- [7] L. Tran, S. R. Ferreira, V. Krelani et al., "Effect of natural fibers on the self-healing capacity of high performance fiber reinforced cementitious composites," in *Proceedings of the 2014 International Conference on Strain-Hardening Cement-Based Composites SHCC 2014: Strain-Hardening Cement-Based Composites*, Dordrecht, Netherlands, 2014.
- [8] C. Zanuy, S. Gonzalo, and D. Ulzurrún, "Impact performance of low-fiber content HPRCC: from material to structural behavior," in *Proceedings of the 2017 International Conference on Strain-Hardening Cement-Based Composites SHCC 2017: Strain-Hardening Cement-Based Composites*, Dresden, Germany, September 2017.
- [9] K. H. Hoang and N. V. Tue, "Comparative flexural and tensile behaviours of ultra-high performance fibre reinforced concrete with different steel fibres," in *Proceedings of the 2017 International Conference on Strain-Hardening Cement-Based Composites SHCC 2017: Strain-Hardening Cement-Based Composites*, Dresden, Germany, September 2017.
- [10] S. Kim, H. Jung, and C. Park, "Effect of steel fiber volume fraction and aspect ratio type on the mechanical properties of SIFCON-based HPRCC," *Structural Engineering and Mechanics*, vol. 65, no. 2, pp. 163–171, 2018.
- [11] M. Tóth, B. Bokor, and A. Sharma, "Anchorage in steel fiber reinforced concrete—concept, experimental evidence and design recommendations for concrete cone and concrete edge breakout failure modes," *Engineering Structures*, vol. 181, pp. 60–75, 2019.
- [12] T. Fukuhara, T. Kanakubo, and A. Ogawa, "Study on the influence of the fiber orientation to the mechanical performance of HPRCC," in *Proceedings of the 14th World Conference on Earthquake Engineering*, Beijing, China, October 2008.
- [13] C. Zanotti, N. Banthia, and G. Plizzari, "Crack growth resistance of concrete-HPRCC interface," in *Proceedings of the 2011 International Conference on Strain-Hardening Cement-Based Composites SHCC 2011: Strain-Hardening Cement-Based Composites*, Rio de Janeiro, Brazil, December 2011.
- [14] M. H. Aliabadi, Q. Li, L. Li et al., "Tensile response and fracture process of high-performance hybrid fiber-reinforced cement composites," *Key Engineering Materials*, vol. 324, pp. 715–718, 2006.
- [15] L. S. Flanders and E. N. Landis, "Experimental measurements of energy dissipation in fiber reinforced ultra high performance concrete under different loading conditions," in *Proceedings of the 2014 International Conference on Strain-Hardening Cement-Based Composites SHCC 2014: Strain-Hardening Cement-Based Composites*, Dordrecht, Netherlands, November 2014.
- [16] B. Jang-Bae, W.-S. Lee, E. Jeon et al., "Experimental study on the mechanical properties of HPRCC with fiber volume fraction of PVA fiber," in *Proceedings of the 2006 Korea Concrete Institute Conference*, pp. 653–656, Seoul, Republic of Korea, 2006.
- [17] D.-Y. Yoo, S. Kim, G.-J. Park, and J.-J. Park, "Residual performance of HPRCC exposed to fire—effects of matrix strength, synthetic fiber, and fire duration," *Construction and Building Materials*, vol. 241, pp. 1–19, 2020.
- [18] Y. Wang, Y. Cao, P. Zhang et al., "Water absorption and chloride diffusivity of concrete under the coupling effect of uniaxial compressive load and freeze-thaw cycles," *Construction and Building Materials*, vol. 209, pp. 566–576, 2019.
- [19] X. Wei, X. Cai, and P. Wu, "EFFECTIVENESS of fabricating high performance fiber reinforced cementitious composite (HPRCC) using high volume steel slag powder," in *Proceedings of the 2017 International Conference on Strain-Hardening Cement-Based Composites SHCC 2017: Strain-Hardening Cement-Based Composites*, Dresden, Germany, September 2017.
- [20] D.-Y. Yoo, J.-J. Park, and S.-W. Kim, "Fiber pullout behavior of HPRCC: effects of matrix strength and fiber type," *Composite Structures*, vol. 174, pp. 263–276, 2017.
- [21] J. Bao, S. Li, P. Zhang et al., "Influence of the incorporation of recycled coarse aggregate on water absorption and chloride penetration into concrete," *Construction and Building Materials*, vol. 239, Article ID 117845, 2020.
- [22] K. G. Kuder and S. P. Shah, "Processing of high-performance fiber-reinforced cement-based composites," *Construction and Building Materials*, vol. 24, no. 2, pp. 181–186, 2010.
- [23] M. Fakharifar, A. Dalvand, M. Arezoumandi, M. K. Sharbatdar, G. Chen, and A. Kheyroddin, "Mechanical properties of high performance fiber reinforced cementitious composites," *Construction and Building Materials*, vol. 71, pp. 510–520, 2014.
- [24] M. Sharbatdar and T. Miyashita, "Tensile stress-strain relationship of high-performance fiber reinforced cement

- composites,” in *Proceedings of the 14th World Conference on Earthquake Engineering*, Beijing, China, 2008.
- [25] S. Gwon and M. Shin, “Direct-tensile and flexural strength and toughness of high-strength fiber-reinforced cement composites with different steel fibers,” *Journal of Asian Concrete Federation*, vol. 2, no. 1, pp. 67–80, 2016.
- [26] D. Kumar and M. Daugevičius, “Influence of HPRCC compressive strength and confinement on concrete,” *Engineering Structures and Technologies*, vol. 11, no. 2, pp. 55–56, 2019.
- [27] R. Nilforoush, M. Nilsson, and L. Elfgren, “Experimental evaluation of tensile behaviour of single cast-in-place anchor bolts in plain and steel fibre-reinforced normal- and high-strength concrete,” *Engineering Structures*, vol. 147, pp. 195–206, 2017.
- [28] J. W. Bao, S. B. Xue, P. Zhang, Z. Dai, and Y. F. Cui, “Coupled effects of sustained compressive loading and freeze-thaw cycles on water penetration into concrete,” *Structural Concrete*, 2020.
- [29] P. Zhang, D. Li, Y. Qiao et al., “Effect of air entrainment on the mechanical properties, chloride migration, and microstructure of ordinary concrete and fly ash concrete,” *Journal of Materials in Civil Engineering*, vol. 30, pp. 1–9, 2018.
- [30] H. Yazici, H. Yigiter, A. S. Karabulut et al., “Utilization of fly ash and ground granulated blast furnace slag as an alternative silica source in reactive powder concrete,” *Fuel*, vol. 87, no. 12, pp. 2041–2407, 2018.
- [31] H. Yazıcı, M. Y. Yardımcı, S. Aydın et al., “Mechanical properties of reactive powder concrete containing mineral admixtures under different curing regimes,” *Construction and Building Materials*, vol. 23, no. 3, pp. 1223–1231, 2009.
- [32] J. Dugat, N. Roux, and G. Bernier, “Mechanical properties of reactive powder concretes,” *Materials and Structures*, vol. 29, no. 4, pp. 233–240, 1996.
- [33] S. L. Yang, S. G. Millard, M. N. Soutsos, S. J. Barnett, and T. T. Le, “Influence of aggregate and curing regime on the mechanical properties of ultra-high performance fibre reinforced concrete (UHPRC),” *Construction and Building Materials*, vol. 23, no. 6, pp. 2291–2298, 2009.
- [34] K. Barnett, T. Mueller, and Y. Ribakov, “Effect of steel fibres on mechanical properties of high-strength concrete,” *Materials & Design (1980–2015)*, vol. 31, no. 5, pp. 2604–2615, 2010.
- [35] S. Xue, P. Zhang, J. Bao, L. He, Y. Hu, and S. Yang, “Comparison of mercury intrusion porosimetry and multi-scale X-ray CT on characterizing the microstructure of heat-treated cement mortar,” *Materials Characterization*, vol. 160, Article ID 110085, 2020.
- [36] P. Zhang, F. H. Wittmann, M. Vogel, H. S. Müller, and T. Zhao, “Influence of freeze-thaw cycles on capillary absorption and chloride penetration into concrete,” *Cement and Concrete Research*, vol. 100, pp. 60–67, 2017.
- [37] Z. Kaiyue, Y. Qiao, P. Zhang, J. Bao, and Y. Tian, “Experimental and numerical study on chloride transport in cement mortar during drying process,” *Construction and Building Materials*, Article ID 119655, 2020.
- [38] Z. Wu, C. Shi, W. He, and D. Wang, “Static and dynamic compressive properties of ultra-high performance concrete (UHPC) with hybrid steel fiber reinforcements,” *Cement and Concrete Composites*, vol. 79, pp. 148–157, 2017.
- [39] G. M. Ren, H. Wu, Q. Fang, and J. Z. Liu, “Effects of steel fiber content and type on static mechanical properties of UHPCC,” *Construction and Building Materials*, vol. 163, pp. 826–839, 2018.
- [40] C. Shi, Z. Wu, D. Wang et al., “A review on ultra high performance concrete: raw materials and mixture design,” *Construction and Building Materials*, vol. 101, pp. 1–13, 2015.
- [41] H. Katrin, E. Denarié, and E. Brühwiler, “Experimental investigation of composite ultra-high-performance fiber-reinforced concrete and conventional concrete members,” *ACI Structural Journal*, vol. 104, pp. 93–101, 2007.
- [42] M. Daugevičius and J. Valivonis, “Concrete and reinforced concrete elements strengthened with HPRCC,” *KSCSE Journal of Civil Engineering*, vol. 22, pp. 2961–2969, 2018.
- [43] Z. Wu, C. Shi, Z. Wu, and D. Wang, “Uniaxial compression behavior of ultra-high performance concrete with hybrid steel fiber,” *Journal of Materials in Civil Engineering*, vol. 17, pp. 1–7, 2016.
- [44] S. Kwon, T. Nishiwaki, T. Kikuta et al., “Development of ultra-high-performance hybrid finer-reinforced cement-based composites (with appendix),” *ACI Materials Journal*, vol. 111, no. 3, pp. 309–318, 2014.
- [45] K. Kobayashi, Y. Asano, and K. Rokugo, “Application of HPRCC as a patching repair material for RC members exposed to chloride attack,” in *Proceedings of the 2011 International Conference on Strain-Hardening Cement-Based Composites SHCC 2011: Strain-Hardening Cement-Based Composites*, Rio de Janeiro, Brazil, December 2011.
- [46] Q. Song, H. Zhao, J. Jia et al., “Pyrolysis of municipal solid waste with iron-based additives: a study on the kinetic, product distribution and catalytic mechanisms,” *Journal of Cleaner Production*, vol. 258, Article ID 120682, 2020.
- [47] A. Hemmati, A. Kheyroddin, M. Sharbatdar, Y. Park, and A. Abolmaali, “Ductile behavior of high performance fiber reinforced cementitious composite (HPRCC) frames,” *Construction and Building Materials*, vol. 115, pp. 681–689, 2016.
- [48] L. Sharbatdar, S. Sun, J. Wang, W. Yang, S. Song, and Z. Fang, “Experimental study of the precursor information of the water inrush in shield tunnels due to the proximity of a water-filled cave,” *International Journal of Rock Mechanics and Mining Sciences*, vol. 130, Article ID 104320, 2020.
- [49] M. Schmidt and E. Fehling, “Ultra high performance concrete research development and application in Europe,” in *Proceedings of the 7th International Symposium on the Utilization of High Strength/High Performance Concrete*, Washington, DC, USA, June 2005.
- [50] M. Rouse Jon and L. Billington Sarah, “Creep and shrinkage of high-performance fiber-reinforced cementitious composites,” *ACI Materials Journal*, vol. 104, no. 2, pp. 129–136, 2007.
- [51] N. T. Tran, T. K. Tran, and D. J. Kim, “High rate response of ultra-high-performance fiber-reinforced concretes under direct tension,” *Cement and Concrete Research*, vol. 69, pp. 72–87, 2015.
- [52] J. Kim, X. Guo, and Y. Zhu, “Repeated penetration of ultra-high performance concrete,” in *Proceedings of the 2014 International Conference on Strain-Hardening Cement-Based Composites SHCC 2014: Strain-Hardening Cement-Based Composites*, Dordrecht, Netherlands, November 2014.
- [53] J. Zhang and Y. Zhao, “The mechanical properties and microstructure of ultra-high-performance concrete containing various supplementary cementitious materials,” *Journal Sustainable Cement-Based Materials*, vol. 6, no. 4, pp. 254–266, 2017.
- [54] D. Wang, C. Shi, Z. Wu, J. Xiao, Z. Huang, and Z. Fang, “A review on ultra high performance concrete: part II. Hydration, microstructure and properties,” *Construction and Building Materials*, vol. 96, pp. 368–377, 2015.

- [55] K. Huang, H. Bian, W. Prince-Agbodjan, and B. Raghavan, "Effect of different types of fibers on the microstructure and the mechanical behavior of ultra-high performance fiber-reinforced concretes," *Composites Part B: Engineering*, vol. 86, pp. 214–220, 2016.
- [56] R. Sovják, P. Máca, and T. Imlauf, "Effect of fibre aspect ratio and fibre volume fraction on the effective fracture energy of ultra-high-performance fibre-reinforced concrete," *Acta Polytechnica*, vol. 56, no. 4, pp. 319–327, 2016.
- [57] D.-L. Nguyen, M. N.-T. Lam, D.-J. Kim, and J. Song, "Direct tensile self-sensing and fracture energy of steel-fiber-reinforced concretes," *Composites Part B: Engineering*, vol. 183, Article ID 107714, 2020.
- [58] Tran, "Determination of the fracture energy of mortar and concrete by means of three-point bend tests on notched beams," *Materials and Structures*, vol. 18, pp. 285–290, 1985.
- [59] National Development and Reform Commission of the People's Republic of China, *Norm for Fracture Test of Hydraulic Concrete: DL/T 5332—2005*, China Electric Power Press, Beijing, China, 2005.
- [60] H. Yokota, K. Rokugo, and N. Sakata, *JSCE Recommendations for Design and Construction of High Performance Fiber Reinforced Cement Composites with Multiple Fine Cracks (HPRCC)*, JSCE, Tokyo, Japan, 1996.
- [61] K. Yu, L. Li, J. Yu, Y. Wang, J. Ye, and Q. Xu, "Direct tensile properties of engineered cementitious composites: a review," *Construction and Building Materials*, vol. 165, pp. 346–362, 2018.
- [62] China National Standards, *Method of Testing Cements—Determination of Strength, GB/T 17671-2005*, China National Standards, Beijing, China, 2005.
- [63] E. Wang and F. H. Wittmann, "The Wedge splitting test, a new method of performing stable fracture mechanics tests," *Engineering Fracture Mechanics*, vol. 35, no. 1–3, pp. 117–125, 1990.
- [64] Ł. Skarżyński and J. Tejchman, "Calculations of fracture process zones on meso-scale in notched concrete beams subjected to three-point bending," *European Journal of Mechanics—A/Solids*, vol. 29, no. 4, pp. 746–760, 2010.
- [65] RILEM-Draft-Recommendation (50-FCM), "Determination of the structure energy of mortar and concrete by means of three-point bend test on notched beams," *Materials and Structures*, vol. 18, pp. 285–290, 1985.
- [66] A. Hillerborg, "Results of three comparative test series for determining the fracture energy of concrete," *Materials and Structures*, vol. 18, no. 107, 1985.
- [67] A. Hillerborg, "The theoretical basis of a method to determine the fracture energy GF of concrete," *Materials and Structures*, vol. 18, no. 4, pp. 291–296, 1985.